



Review

# A Review on Tribocorrosion Behavior of Aluminum Alloys: From Fundamental Mechanisms to Alloy Design Strategies

Zhengyu Zhang, Raja Shekar Bhupal Dandu, Edwin Eyram Klu and Wenjun Cai \*

Department of Materials Science and Engineering, Virginia Polytechnic Institute and State University, Blacksburg, VA 24061, USA

\* Correspondence: caiw@vt.edu

**Abstract:** Tribocorrosion, a research field that has been evolving for decades, has gained renewed attention in recent years, driven by increased demand for wear- and corrosion-resistant materials from biomedical implants, nuclear power generation, advanced manufacturing, batteries, marine and offshore industries, etc. In the United States, wear and corrosion are estimated to cost nearly USD 300 billion per year. Among various important structural materials, passive metals such as aluminum alloys are most vulnerable to tribocorrosion due to the wear-accelerated corrosion as a result of passive film removal. Thus, designing aluminum alloys with better tribocorrosion performance is of both scientific and practical importance. This article reviews five decades of research on the tribocorrosion of aluminum alloys, from experimental to computational studies. Special focus is placed on two aspects: (1) The effects of alloying and grain size on the fundamental wear, corrosion, and tribocorrosion mechanisms; and (2) Alloy design strategies to improve the tribocorrosion resistance of aluminum alloys. Finally, the paper sheds light on the current challenges faced and outlines a few future research directions in the field of tribocorrosion of aluminum alloys.

**Keywords:** corrosion; wear; tribocorrosion; aluminum alloys; alloy design



**Citation:** Zhang, Z.; Dandu, R.S.B.; Klu, E.E.; Cai, W. A Review on Tribocorrosion Behavior of Aluminum Alloys: From Fundamental Mechanisms to Alloy Design Strategies. *Corros. Mater. Degrad.* **2023**, *4*, 594–622. <https://doi.org/10.3390/cmd4040031>

Academic Editor: Kevin Ogle

Received: 30 July 2023

Revised: 28 September 2023

Accepted: 11 October 2023

Published: 18 October 2023



**Copyright:** © 2023 by the authors. Licensee MDPI, Basel, Switzerland. This article is an open access article distributed under the terms and conditions of the Creative Commons Attribution (CC BY) license (<https://creativecommons.org/licenses/by/4.0/>).

## 1. Introduction

Tribocorrosion is a material degradation process caused by the combined effect of wear and corrosion [1,2]. The complexity of tribocorrosion lies in the fact that the chemical and mechanical attacks are not independent of each other but often act synergistically to cause accelerated failure [3–5]. The synergetic effect is most prominent for passive metals. Passive metals, which include important engineering metals such as stainless steels, aluminum (Al), and titanium alloys, spontaneously form a thin oxide film (passive film) when in contact with oxygen or water [6]. This passive film, sometimes only a few atomic layers thick, acts as a critical protective barrier against corrosion [2,6]. When mechanical wear occurs during corrosion, the passive film can be locally destroyed at the contacting asperities, with the ensuing depassivation leading to rapid localized corrosion and early component failure [2,3,7–9]. A better understanding of the tribocorrosion response of passive metals is required to extend the durability of these technologically important metals in complex service conditions. The paper begins by briefly reviewing the history and research trends in this area, followed by a discussion of the fundamental mechanisms of alloying and grain size effects on the wear, corrosion, and tribocorrosion behavior, elucidating the interplay between mechanical contact and electrochemical processes in Al alloys. It then explores the various alloying design strategies that simultaneously improve wear and corrosion resistance, hence the tribocorrosion resistance. Finally, we conclude by addressing the need for the integration of multiscale modeling, machine learning, and experimental techniques as a promising future avenue for gaining insights into complex tribochemical interactions. This review primarily focuses on alloying design, while coatings and other surface modifications of metals and alloys are beyond the scope of this article. Readers

interested in tribocorrosion of coatings may refer to several papers such as [10–12] for a focused review on the performance of coatings under combined wear and corrosion conditions.

## 2. Brief History and Literature Survey from the Past Five Decades

A literature survey on Scopus database, searching for “tribo-corrosion OR tribocorrosion” in the article title, abstract, and keywords from 1973–2023 results in 1722 papers. The keywords “tribocorrosion” and “tribo-corrosion” are often used interchangeably by various research groups. Other most commonly used keywords include “corrosion,” “wear of materials,” “friction,” “tribology,” etc.

Figure 1a shows the number of papers in this field as a function of year, where most papers have been published within the past two decades. Early pioneers on tribocorrosion include Neukirchner, J and Wunsch, F. et al. in the 1970–1980s. However, these works were written in German, hence they received relatively little citation internationally. One of the early papers that really sparked international interest is a 1993 Wear paper [13] by Mischler, S., Rosset, E., Stachowiak, G.W., and Landolt, D. In this study, wear and corrosion were not performed simultaneously. Instead, tribocorrosion tests were conducted by corroding a sample after a dry wear test. Specifically, the study involved monitoring the coefficient of friction, material loss rates, and surface morphology of iron when rubbed against alumina in sulphuric acid solutions ranging from 2 M to 18 M. The key results are interesting but not surprising to today’s readers: The research revealed that the combination of wear and corrosion can significantly impact the material removal mechanisms compared to static corrosion conditions.

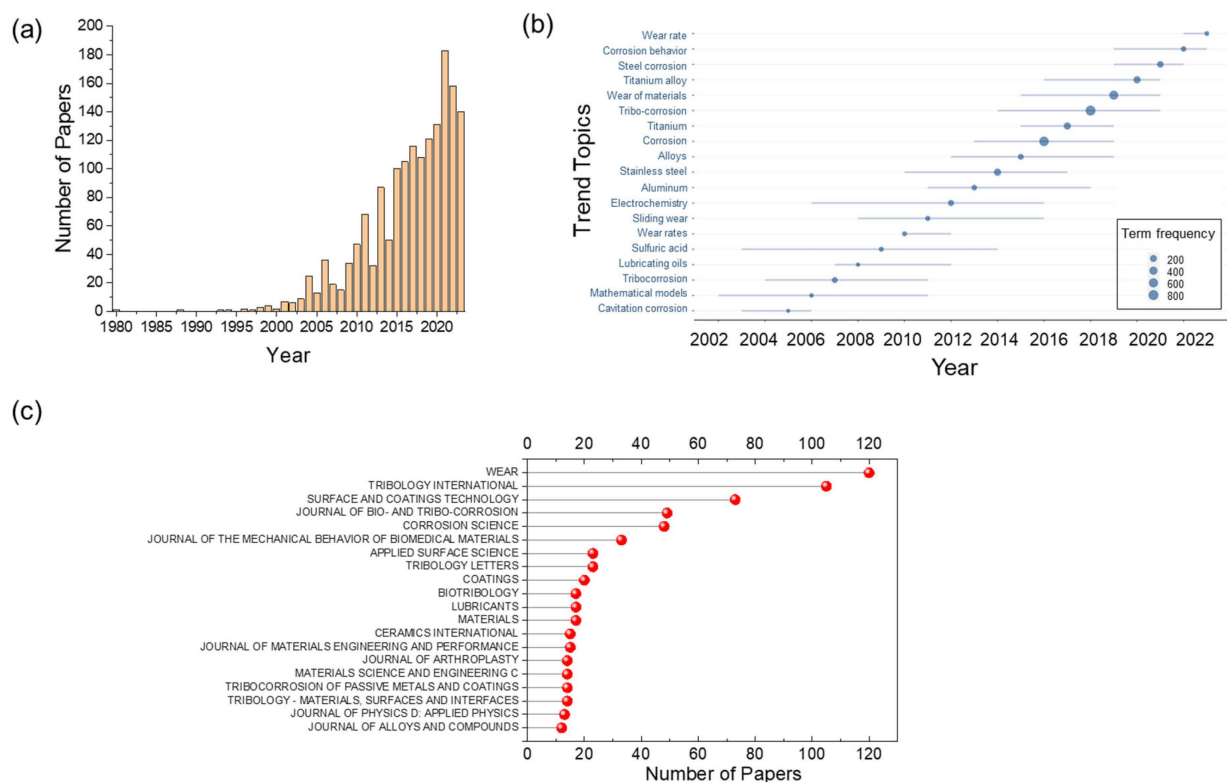


**Figure 1.** Summary of literature review of tribocorrosion papers published from 1973–2023. (a) Annual production, (b) Trending topics, and (c) Most relevant journals.

Figure 1b shows the trending topics in the field of tribocorrosion within the last two decades, where steel, titanium, and aluminum alloys are among the most popular materials studied. Figure 1c shows the popular journals that have published tribocorrosion-related papers, with Wear, Tribology International, and Surface and Coatings Technology as the

top three. Over the years, several papers summarize and review important experimental methods and fundamental mechanisms of tribocorrosion. For example, Landot et al. [4] provided an extensive overview on the electrochemical methods in tribocorrosion studies both theoretical and experimental. The authors expounded on the kinetics that occur during the tribocorrosion process, and they highlighted critical electrochemical conditions and parameters that should be considered when performing tribocorrosion experiments [14]. López-Ortega et al. [15] provide a detailed review of the literature relating to the test procedures and standards employed to assess tribocorrosion behavior of passive materials, such as ASTM G119 [16] and the UNE 112086 [17] standard. The specific mechanism for tribocorrosion and wear-corrosion synergy remains under active research because it depends on various materials and testing parameters [1–3]. It is often believed that the combination of wear and corrosion does not result in a mere additive effect of each process. Instead, a synergistic effect occurs, which may further increase or sometimes decrease the overall material loss. Maher et al. [18] provided a thorough review of the wear-corrosion interaction on stainless steels, which takes account of the effects of the stainless-steel type, temperature, pH, solid concentration, the eroded particle size and shape, etc. Apaza-Bedoya et al. [19] reviewed the tribocorrosion of titanium-based dental implant connections and discuss the degradation caused by the wear and corrosion processes in the oral cavity. Recently, a review paper by Abolusoro and Akinlabi [20] provides an overview of tribocorrosion behaviour of Al Alloys by categorizing the mechanism as a function of various parameters such as heat treatment, corrosion inhibitors, and the presence of coatings and surface treatment.

In addition to journal papers, the book titled *Tribocorrosion of passive metals and coatings* (2011) by Dieter Landolt and Stefano Mischler provides a comprehensive introduction and review of current research on the tribocorrosion of passive metals and coatings, from the design of tribocorrosion test equipment, data evaluation, to design optimization of materials' properties for tribocorrosion systems. Another recent book titled *Tribocorrosion: Fundamentals, Methods, and Materials* (2021), edited by Arpith Siddaiah, Rahul Ramachandran, and Pradeep Menezes covers recent developments in both the experimental and computational aspects of tribocorrosion, encompassing fundamental principles in tribology and electrochemistry, as well as examination setups, procedures, electrochemical techniques, and additional topics. In addition, a book chapter on *Tribocorrosion: Definitions and Relevance* (2020) [21] by Anna Igual Munoz, Nuria Espallargas, and Stefano Mischler as part of the Springer Briefs in Applied Sciences and Technology book series provides readers with a concise introduction of tribocorrosion in simple words.

The family of materials whose tribocorrosion properties are important include various engineering metals such as steel, titanium, and aluminum alloys. Other commonly studied materials include nickel [22–24], magnesium [25–27], and high entropy alloys [28–33]. The most commonly studied electrolytes include NaCl solutions/seawater [34,35], acidic HCl and H<sub>2</sub>SO<sub>4</sub> solution [36–39], alkaline NaOH solutions [37,40], and solutions utilized at human body temperature (37 °C), such as simulated body fluid (SBF) [41,42], phosphate-buffered saline (PBS) [33,43,44], Hank's solution (HBSS) [45,46], and Ringer's solution [47,48]. For brevity, this paper mainly focuses on the tribocorrosion behavior of Al alloys in NaCl solutions. Among those relevant studies, the tribocorrosion behavior of Al alloys are often studied due to three types of effects: (1) The material parameters, such as alloy composition [49], fraction of reinforcing particles [50–55], and heat treatment [56]; (2) The corrosion testing parameters, such as applied current/potential [56], corrosion inhibitor [57,58], and electrolyte composition [59,60]; and (3) The wear testing parameters, such as applied load [59,61] and speed [61,62]. For the material parameter effects, Ferreira et al. [50] investigated the effects of spatial distribution of reinforcing particles (e.g., Al<sub>3</sub>Ti and Al<sub>3</sub>Zr) on the tribocorrosion resistance of Al-5 wt.% Ti and Al-5 wt.% Zr in 0.6 M NaCl solution. They found that higher surface hardness results in a lower tribocorrosion rate. Similarly, Jamaati et al. [51] showed that in Al/Al<sub>2</sub>O<sub>3</sub> composite material, a more uniform distribution and higher concentration of the reinforcing Al<sub>2</sub>O<sub>3</sub> particles result

in better corrosion resistance of Al in 0.1 wt.% NaCl solution. In addition to material modification via reinforcing particles, heat treatment was also found to greatly affect the tribocorrosion behavior of Al alloys. Xu et al. [56] investigated the effects of T4 and T5 heat treatment on the tribocorrosion behavior of 7B05 Al alloy (Al alloy with 5.00–6.50 wt.% Zn, 0.05–1.0 wt.% Mg, and trace Mn, Cr, Zr, Ti, Cu, Fe, Si) in artificial seawater. It was discovered that T5 treatment results in a more uniform grain size and banded precipitate as compared with the T4 sample, which leads to better corrosion resistance. However, T4 treatment produced more uniform distribution of precipitated phase and higher hardness than T5, eventually resulting in better tribocorrosion resistance than T5 treatment.

In terms of the effects of corrosion testing parameters, increasing the applied potential in the more anodic direction often results in significant increase in the tribocorrosion rate of Al alloys due to higher intensity of corrosion reaction and corrosion-induced wear [56,60]. For example, the corrosion of 7B05 Al alloy after T4 and T5 heat treatment was found to be more aggravated at the anode potential, resulting in higher surface roughness than that under cathodic or open circuit potentials (OCP) [56]. Similarly, Chen et al. [63] show that the total tribocorrosion material loss of LY12 Al alloy increased with applied potential. Specifically, as shown in Figure 2a, the pure wear loss ( $V_{M0}$  in Figure 2a) remained relatively constant, while  $V_C$ , the total material loss caused by pure corrosion, and  $\Delta V_M$ , the corrosion-induced wear, became increasingly larger at the more anodic potentials. The presence of corrosion inhibitor [57,58] and electrolyte composition [59,60] also affects the overall tribocorrosion rate.

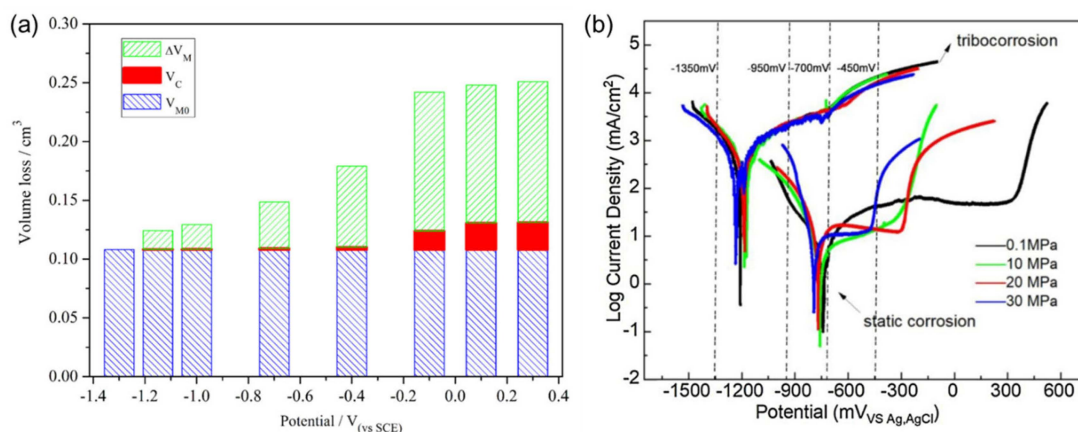


**Figure 2.** (a) Material loss from pure wear ( $V_{M0}$ ), pure corrosion ( $V_C$ ), and corrosion-induced wear ( $\Delta V_M$ ) of Al Alloy in artificial seawater at different applied potentials (Replotted from Ref. [63]). (b) Potentiodynamic polarization curves of 7075-T6 alloy under various hydrostatic pressure levels in a 3.5 wt.% NaCl solution (Replotted from Ref. [64]).

Corrosion inhibitors such as sodium octanoate [57] and zinc phosphate [58] were found to reduce tribocorrosion rate of Al alloys in NaCl solutions due to the formation of a surface barrier that not only limit mass and charge transfer to reduce corrosion, but also lowers surface friction to reduce wear. Liu et al. [60] showed that the tribocorrosion rate of 7075-T6 Al alloy is higher in seawater than deionized water and ethanal. For wear testing parameters, increasing the applied load and scratching speed were found to increase the total tribocorrosion material loss of Al alloys [61,62]. Li et al. [64] showed a similar trend for tribocorrosion of Al in deep ocean when the applied load is not uniaxial, but rather hydrostatic. Interestingly, they also found that as hydrostatic pressure rises, the passivation duration diminishes (Figure 2b), suggesting that the formation of the passive film on Al alloy is impeded when subjected to high hydrostatic pressure. When experiencing tribocorrosion, the passivation period within the Al alloy's polarization curve vanishes (Figure 2b), leading to a faster anodic dissolution rate compared to static corrosion.

### 3. Effects of Alloying and Grain Size on Wear Resistance of Al Alloys

#### 3.1. Alloying Effects

Alloying leads to increased hardness and improved wear resistance of metals in most cases per Archard's law [65,66]. In addition to hardness increment, proper alloying additions can significantly lower the grain boundary energy and stabilize ultrafine microstructures in the tribolayer to suppress stress-assisted grain growth and improve the surface hardness and the overall wear resistance [67]. For example, Jiru and Sing [68] showed that surface alloying of Al with manganese (Mn) improved surface hardness, lowered the coefficient of friction, and reduced wear rate of aluminum by 30%. Dubourg et al. [69] found that the wear rate of Al–Cu alloys decreased with increasing Cu concentration from pin-on-disk wear tests under 2–4 N load and 0.05–0.2 m/s sliding speed (Figure 3a). Du et al. [70] demonstrated a similar behavior in additively manufactured Al-5 wt.%Cu alloys via laser powder bed fusion, as shown in Figure 3c,d, where the addition of ~1.5 wt.% Ti results in a reduction of wear rate from to  $9.79 \times 10^{-4} \text{ mm}^3/(\text{N}\cdot\text{m})$  to  $3.05 \times 10^{-4} \text{ mm}^3/(\text{N}\cdot\text{m})$  after ball-on-disk wear tests under 10 N load for a sliding time of 30 min. In emerging high-entropy alloys, the wear coefficient of  $\text{Al}_x\text{CoCrCuFeNi}$  alloys with 9–28.6 at.% Al decreases as the aluminum content increases [71]. Specifically, the wear coefficient of high aluminum content alloy is about one seventh of that of low aluminum content counterpart due to a change of the wear mechanism from delamination wear to oxidative wear with increasing aluminum content. Yu et al. [72] found that AlCoCrFeNiTi0.5 shows better dry wear resistance than wear-resistant steel AISI 52100 due to nano-sized Fe–Cr solid solution and Al–Ni–Ti rich intermetallic phases. However, the opposite has also been reported in terms of both hardness and wear resistance. For example, the addition of Zr, Mn, V, Cr, and other micro-elements to 7xxx series aluminum alloy (Al–Zn–Mg) results in a decrease of hardness [73]. De Rosso et al. [74] showed that the wear rate of Al–Si alloys decreases at higher Cr content but lower Si contents due to the smaller secondary dendritic arm spacings and higher hardness.

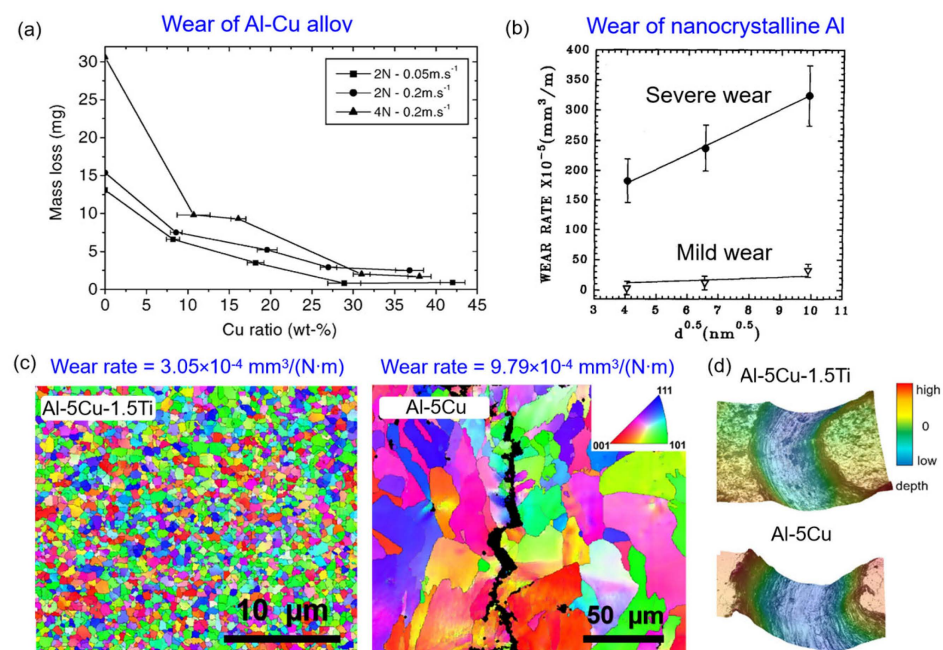


**Figure 3.** (a) Mass loss evolution of Al–Cu alloy with various Cu concentrations from pin-on-disk wear tests over 500 m sliding distance (Replotted from Ref. [69]). (b) Wear rate versus square root of grain size ( $d^{0.5}$ ) of nanocrystalline Al under severe and mild wear (Replotted from Ref. [75]). (c) EBSD maps and (d) 3D profiles of wear track of additively manufactured Al-5 wt.%Cu-1.5 wt.%Ti and Al-5 wt.%Cu samples after ball-on-disk wear tests under 10 N load for a sliding time of 30 min. (Replotted from Ref. [70]).

From a more general point of view, it is interesting to note that subsurface microstructures tend to be driven into a non-equilibrium status under constant wear and friction, leading to dynamically self-organized microstructures similar to those in ball-milling [76] or under ion irradiation [77]. In non-equilibrium systems, when several competing processes are present (such as dislocation accumulation due to sustained plastic deformation vs. stress-assisted grain growth and dynamic recovery), a steady state and equilibrium microstructure is not always achieved [78]. For example, Kasai et al. [79] performed wear tests of pin sliding against a brass disc in air and found that the Kelvin probe signal on the surface is nearly periodic, indicating the periodic change of surface chemistry and structure and an absence of steady state. Another example of the lack of a steady state in wear is the well-known stick-slip frictional behavior observed in many elastomers when subjected to low sliding velocities and/or high normal pressures [80]. However, non-equilibrium surface microstructures, such as supersaturated solid solutions has also been reported in the tribolayer [81], where the level of supersaturation is far beyond the equilibrium solubility limit, similar to those observed during mechanically alloying and severe plastic deformation [82,83].

Alloying effects on wear of Al is complicated due to the various phase distribution and microstructure formation in different alloying systems. Generally speaking, higher alloy concentration leads to improved wear resistance but an **optimum alloy concentration for the best wear resistance is not known a priori**. For example, Jasim and Dwarakadasa [84] showed that the wear rate of Al-Si alloys decreases with Si content up to the eutectic composition and did not depend on the initial microstructure or the distribution of the silicon phase. Similar behavior is also observed in Al-Cu [69], Al-Cu-Fe [85], Al-Sn [86], etc. From a more general point of view, it is interesting to note that subsurface materials tend to be driven into a non-equilibrium status under constant wear and friction, leading to dynamically self-organized microstructures similar to those in ball-milling [76] or under ion irradiation [77]. In non-equilibrium systems, when several competing processes are present (such as dislocation accumulation due to sustained plastic deformation versus stress-assisted grain growth and dynamic recovery), a steady state is not always achieved [78]. As a result, a single optimum alloy concentration may not always exist.

### 3.2. Grain Size Effects

In addition to alloying, another important tunable microstructure feature is grain size [87]. Refined grain size often leads to increased hardness and improved wear resistance, per Archard's law [65], especially when abrasive wear is the dominating mechanism. For example, nanocrystalline Al with ~16 nm grain size exhibits a reduction of friction coefficient by about 55% compared to microcrystalline Al [75]. Farhat et al. [75] investigated the friction and wear characteristics of nanocrystalline Al as a function of grain size. They found that both mild and severe wear increased linearly with the square root of grain size, following a modified Archard-type of relationship, as shown in Figure 3b. However, when high stress is applied during wear, the large amount of plastic deformation at the contact surface leads to stress-assisted grain growth due to the high mobility of nanocrystalline grain boundaries and results in wear resistance higher than what would be expected based on hardness alone [8,88].

It should be pointed out that since these wear tests were performed at room temperature and moderate sliding speed, frictional heating was ruled out as the driving force for the observed grain growth [8]. Another deviation from Archard's law is that the optimum grain size for wear resistance does not coincide with the grain size for the highest hardness at the Hall-Petch crossover. The **optimum grain size for wear is not known a priori**. For example, Jeng et al. [88] showed that the hardness of nanocrystalline Ni reaches a maximum at grain size of 15 nm, while the optimum wear rate is reached at grain size of 30 nm. Further reducing the grain size does not alter the wear rate much. From a more general point of view, it is interesting to note that subsurface materials tend to be driven into a non-equilibrium status under constant wear and friction, leading to dynamically

self-organized microstructures similar to those in ball-milling [76] or under ion irradiation [77]. In non-equilibrium systems, when several competing processes are present (such as dislocation accumulation due to sustained plastic deformation versus stress-assisted grain growth and dynamic recovery), a steady state is not always achieved [78]. As a result, a single optimum grain size may not always exist.

#### 4. Effects of Alloying and Grain Size on Corrosion Resistance of Al Alloys

##### 4.1. How Does Alloying Affect Corrosion of Al Alloys?

Al and Al alloys form an amorphous semiconducting passive film in neutral (pH 4–9) solutions [89]. This passive film is still vulnerable to the local attack of different halide ions. The adsorption of halide ions on the surface leads to localized breakdown of the passive film and eventually leads to pitting and crevice corrosion of Al. Unlike in wear-only conditions, alloying may affect corrosion resistance of Al in different ways depending on the specific alloying elements, as reviewed by Szklarska-Smialowska [90]. Small quantities of Sn, In, Hg, Ga, and Zn are detrimental to Al corrosion, as they reduce the passive potential region and shift the corrosion and pitting potentials in the negative direction [91]. Thus, these transition metals (TMs) lead to high anodic current density and uniform active surface corrosion. Other TMs, such as Cu, Mo, Mn, W, Nb, Cr, Ta, V, and Zr, improve corrosion resistance and decrease pitting susceptibility of Al by increasing the overpotential for anodic dissolution and decreasing metastable pit initiation and growth rates [92]. For example, Mraied et al. [93] showed that increasing the Mn concentration of Al–Mn alloys from 0–20.5 at.% resulted in higher corrosion resistance and the formation of much smaller pit sizes at higher Mn content, as shown in Figure 4a. Unlike pure Al (A0), which clearly showed through thickness circular “pits” of  $\sim 120\ \mu\text{m}$  in diameter after 24 h of immersion in 0.01 M NaCl solution, Al–Mn alloys (A5–A20 in Figure 4a) did not reveal any marked localized attack after 108 h of immersion. Instead, a network of conspicuous grooves developed on alloy A20 with  $\sim 100\ \text{nm}$  in depth. Corrosion mechanisms of Al has been reviewed from the perspectives of acid–base interactions [94], chloride ion interactions with surface oxide film [95], critical steps involved in localized corrosion and stressed corrosion [96], and the effects of corrosion inhibitors [97], etc. Specifically, the review by Olugbade [98] discusses the effects of plastic deformation, including ultrasonic shot peening, equal-channel angular processing, constrained groove pressing, etc., and addresses the impacts of deformation on corrosion, which shares some similarity with tribocorrosion for the wear-induced gradient subsurface microstructure [99].

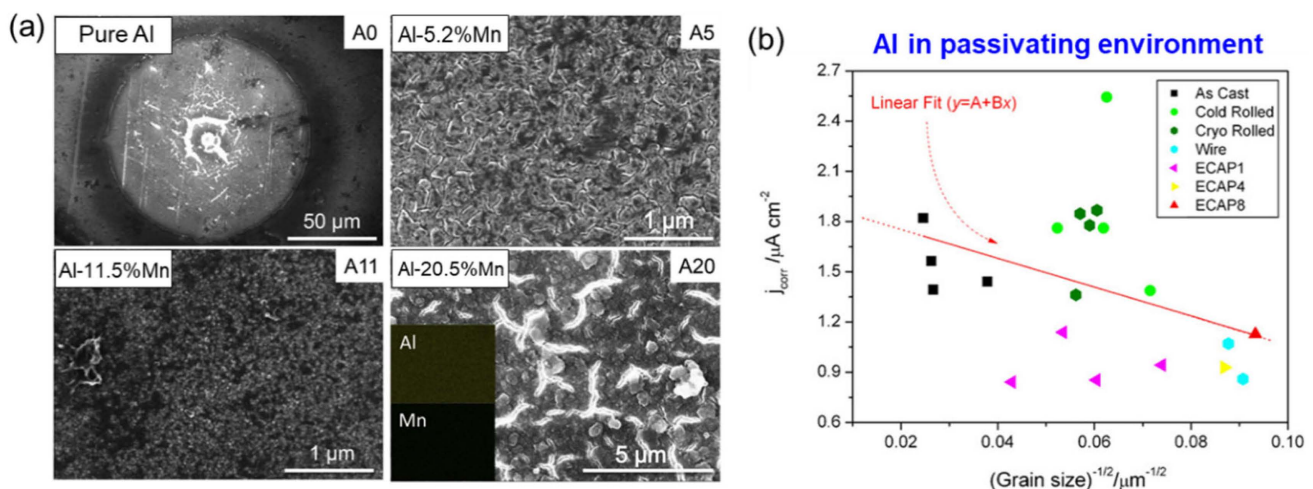


**Figure 4.** (a) SEM micrographs of corroded surfaces of Al alloys after immersion in 0.01 M NaCl solution for 24 h for pure Al and 108 h for all Al–Mn alloys (Replotted from Ref. [93]). (b) Corrosion current and grain size of Al follows a Hall–Petch type relationship (Replotted from Ref. [100]).

#### 4.2. Does Corrosion Resistance Depend on Grain Size?

Unlike in wear-only conditions, grain size may affect corrosion resistance in different ways depending on the specific corrosion mode. For the technologically important case of corrosion resistance of passive metals, it is thought that grain size influences corrosion resistance by affecting the rate of ion transport through the passive film, as well as the passive film dissolution rate [101]. The nanocrystalline materials involve a much higher linear boundary intersection density at the surface compared to their microcrystalline counterparts. This high density of grain boundaries leads to higher average surface reactivity through increased electron state density and diffusional defect transport. Those factors are believed to lead to higher stability and better adherence of the passive film on nanocrystalline materials [101]. For passive metals, including Al [100,102], Ti [103], Ti alloys [104], and steel [105,106], it has been shown that indeed reducing grain size leads to improved corrosion resistance. However, it should be pointed out that these results are drawn from a wide variety of test conditions that often do not isolate the effect of other microstructural changes imparted by the grain refining process from the effect of grain size decrease alone. These microstructural changes include, among others, a secondary phase refinement, texture evolution, and residual stress build-up. As experimental focus and conditions vary among various studies, reported findings on grain size effects to date often tend to be contradictory. Orłowska et al. [107] studied the effect of grain size on the corrosion behavior of commercially pure Al processed by multi-turn equal channel angular pressing and upsetting. Despite the significant change of grain size from  $\sim 11 \mu\text{m}$  to  $\sim 669 \text{ nm}$  after severe plastic deformation, grain refinement was found to show negligible effects on the pitting behavior. Instead, Fe-containing particles, which are pit nucleation sites, are determined to be the crucial factor for the observed corrosion behavior. Since there is no difference in size and number of these particles after the severe plastic deformation, the electrochemical parameters showed very similar values for samples with different grain sizes. Olugbade reviewed the corrosion rate of Al alloys processed by equal channel angular pressing (ECAP) and summarized that the corrosion current density generally decreases at smaller grain size. Ralston et al. [100] studied corrosion resistance of high-purity Al with grain sizes from  $\sim 100$  to  $2000 \mu\text{m}$  processed using different plastic deformation methods. They found, albeit with considerable remaining uncertainty, that corrosion resistance increased with the reciprocal square root of grain size in a manner analogous to the Hall–Petch relationship, as shown in Figure 4b. Similar behavior was found for nanocrystalline Al and Al alloys [102,108,109]. However, the opposite behavior has been reported by others [110,111]. Eizadjou et al. [110] showed that Al with grain size of  $\sim 380 \text{ nm}$  produced by accumulative roll bonding (ARB) was more susceptible to corrosion than coarse grained Al with  $\sim 33.8 \mu\text{m}$  grain size, a result that was interpreted as due to a high density of defects and inhomogeneities in the passive film. Similar contradictory results have also been reported in Ti alloys [104,112] and Mg alloys [113,114].

### 5. Tribocorrosion Behavior and Mechanisms of Al Alloys

The complexity of tribocorrosion lies in the fact that chemical and mechanical degradation mechanisms are not independent of each other. A combination of mechanical and chemical attack often (but not always) leads to accelerated failure due to synergetic effects. Thus, the total material loss  $T = W_0 + C_0 + S$ , where  $W_0$  is the material loss due to mechanical wear in the absence of corrosion,  $C_0$  is the material loss resulted from corrosion in the absence of wear, and  $S$  is the material loss due to wear–corrosion synergy [3,4]. The synergetic effect is most prominent for passive metals. Passive metals, which include important engineering metals such as aluminum, titanium, and stainless steels, spontaneously form a thin oxide film (passive film) when in contact with oxygen or water [6]. This passive film, sometimes only a few atomic layers thick, acts as a critical protective barrier against corrosion [2,6]. When mechanical wear takes place during corrosion, the passive film can be locally destroyed at the contacting asperities, with the ensuing depassivation leading to rapid localized corrosion and early component failure [2,3,7–9]. It should be noted that the

interaction between corrosion and wear can also be antagonistic, where the synergy term is negative [10]. However, the occurrence of a corrosion film that is either soft or weakly attached can lead to reduced contact stress and wear [10,115]. On the other hand, the worn surface frequently displays swift development of a passive film, which further reduces corrosion [115].

In Figure 5, we present an original schematic diagram that visually represents the various relevant mechanical and electrochemical events that occur during tribocorrosion of passive metals. During sliding wear by an indenting agent, the native passive film on the alloy is disturbed and partially removed. The indenter material is often a harder material than the metal, such as diamond, alumina ( $\text{Al}_2\text{O}_3$ ), and tungsten carbide (WC). Highly reactive base metal is exposed, leading to a high local anodic current density transient, supported by a matching increase in the surrounding cathodic current density but over a larger area (of size largely determined by the macrocell ohmic coupling and, thus, by the electrolyte resistivity [116]) and, hence, not strongly polarized. In an Al alloy, the re-grown film develops with kinetics that is accelerated by the high density of point defect sinks and sources at the intersection between grain boundaries and the film/metal interface [6]. That desirable effect may be counteracted, to some extent, by an increase in the overall passive dissolution anodic current and pitting tendency elsewhere in the passive film. There, grain boundary intersections and related film defect injection and sinks could enhance the rate of steady-state transport processes and possibly also adversely increase the electronic donor/acceptor density, thereby increasing the rate of the cathodic reaction. Opposing effects also exist when considering that the alloying elements in the substrate are expected to improve tribological resistance by increasing hardness. However, the enhanced grain boundary transport of alloying elements and additional mechanical deformation mechanisms such as grain boundary sliding and grain rotation may begin to become important at higher alloying concentrations and finer grain sizes. Wear debris, which may aggravate passive film removal when trapped by the indenter, can be another factor to improve or degrade tribocorrosion resistance with increasing alloy concentration.

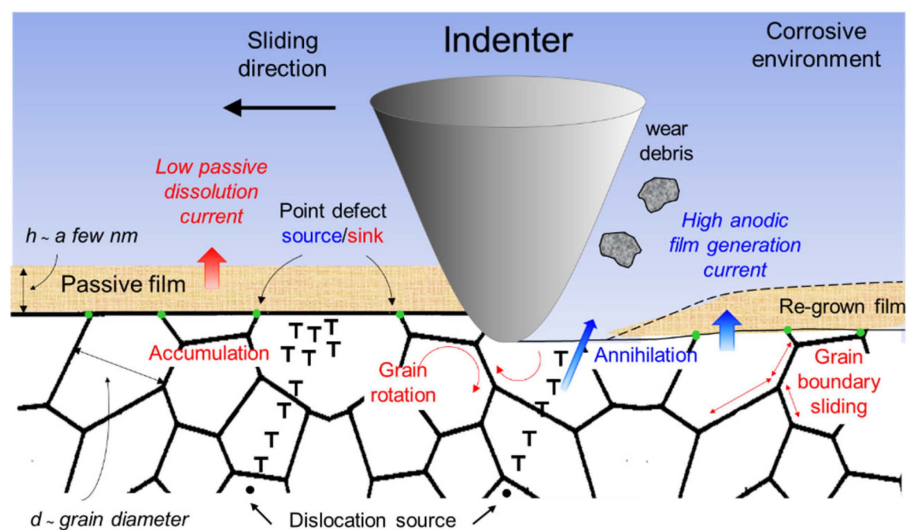


**Figure 5.** Schematic summary of relevant mechanisms influencing the tribocorrosion performance of passive metals in corrosive environment. This original schematic was created by the authors for this study.

## 6. Tribocorrosion Resistance of Al Alloys

Most commercial Al alloys are precipitation-hardened to impart good strength and wear resistance, but none of them have very good resistance against localized corrosion. The presence of precipitation and secondary particles strengthens the material, but, at the

same time, enhances corrosion by catalyzing oxygen reduction, increasing the alloy corrosion potential and localizing the electrochemical activity due to chemical inhomogeneity from the Al matrix [89]. Recent studies show that alloying additions can increase the pitting potential of Al provided that the alloying element is retained in solid solution [92,117–119]. For example, age-hardened 2000 series Al alloys (with Cu as the major alloying element) exhibit poor corrosion resistance [89], but Kim et al. observed an ennoblement of pitting potential with increasing Cu content in Al–Cu solid solutions [92,117]. Thus, to simultaneously improve wear and corrosion resistance, the formation of chemically and physically homogeneous Al alloys is crucial.

Currently, there is no unified theory relating grain size to the tribocorrosion resistance of engineering alloys. Research effort in this area has been very limited so far. A quick search of *Scopus* using topic key words of “tribocorrosion + grain size” led to only 37 results from 1900 to July 2023, as compared to 6,522 results for “wear + grain size” and 8725 for “corrosion + grain size.” Nevertheless, some of these studies [112,120–122] indicate that smaller grain size increases tribocorrosion resistance, while one suggests the opposite trend [123].

## 7. How to Design Tribocorrosion-Resistant Al Alloys?

A comprehensive understanding of how alloying and grain size of Al alloys influences tribocorrosion response is largely lacking. Current research in this area is very limited in scope. Abundant literature exists pertaining to the possible alloying and grain size effects on wear and corrosion resistance, but fewer attempts have been made to combine knowledge based on these two separated field towards a better understanding of tribocorrosion. This has directly challenged the design of tribocorrosion-resistant Al alloys. In terms of alloying effects, higher alloying content tends to improve wear resistance, although the optimum alloy concentration is not known *a priori* due to complicated dynamic microstructure evolution in the tribolayer. For corrosion, several alloy elements increase the pitting potential of Al provided that the alloying elements are retained in solid solution. In terms of the grain size effects, smaller grain sizes tend to improve wear resistance, although the optimum grain size is not known *a priori* due to complicated dynamic microstructure evolution in the tribolayer. For corrosion, contradictory results have been reported due to the oversimplification of grain size effect in many published studies.

Figure 6 summarizes the wear rate versus corrosion rate of Al-based alloys, including 1000-, 5000-, and 6000-series Al alloys, Al-based bulk metallic glass (BMGs), and Al-based high-entropy alloys (HEAs). Comparing the behavior of 1000-series (commercial Al) versus 5000- and 6000-series alloyed Al, it can be seen that alloying indeed enhanced wear resistance, but compromised corrosion resistance. Al–HEA and Al–BMGs exhibit much better strength and wear resistance compared to commercial Al alloys. However, their corrosion behavior is quite widespread. As summarized above, most commonly used metal design strategies such as alloying and grain size control cannot be directly applied to design tribocorrosion resistance. Next, three alloy design strategies to effectively improve the tribocorrosion resistance of Al alloys are discussed based on our recent studies, namely, the formation of (1) Supersaturated solid solutions, (2) Nanostructured multilayers, and (3) Controlled crystallographic texture.

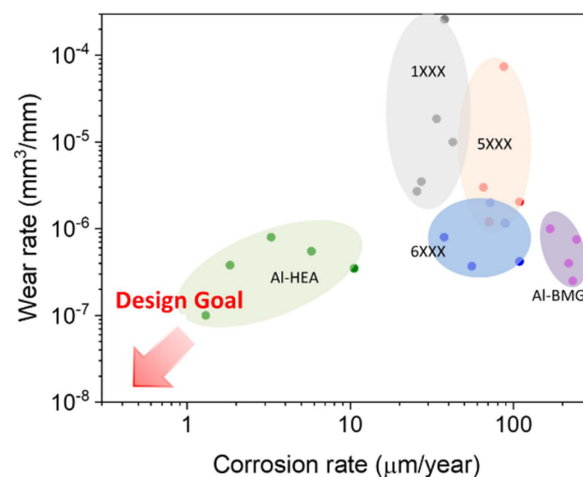


**Figure 6.** Summary of wear rate versus corrosion of Al-based alloys from literature review. Plotted using data obtained from Refs. [124,125]. Al-HEA represents  $\text{Al}_x\text{Co}_{1.5}\text{CrFeNi}_{1.5}\text{Ti}_y$  high-entropy alloys, Al-BMG represents  $\text{Al}_{90.05}\text{Y}_{4.4}\text{Ni}_{4.3}\text{Co}_{0.9}\text{Sc}_{0.35}$  bulk metallic glasses, and 1xxx, 5xxx, and 6xxx represents different series of Al alloys.

### 7.1. Strategy 1: Formation of Supersaturated Solid Solutions

Alloying is an effective way to improve materials wear resistance by increasing its strength, which is indeed what most commercial alloys are doing. Therefore, you are decreasing the wear rate. Unfortunately, the precipitates are strengthened material that also accelerate corrosion due to the galvanic coupling with the aluminum matrix. So, a decreased wear rate is at the expense of increased corrosion rate. For example, a survey of Al-X binary system shown in Figure 7 indicates that, in general, hardness (H) and pitting potential ( $E_{\text{pit}}$ ) increase with alloying concentration for a wide range of alloying elements. However, due to the galvanic coupling effects, the corrosion current ( $i_{\text{corr}}$ ) does not show a clear dependence on alloying concentrations (Figure 7c,d).

To simultaneously minimize both wear and corrosion, one effective microstructure design strategy includes forming a solid solution alloying to combat the trade-off between wear and corrosion. However, typically solid solution strengthening results in poorer mechanical properties than precipitation hardening [126]. In precipitation hardened alloys, the type, size, and distribution of intermetallic are vital for their tribocorrosion behavior [56]. To further enhance the mechanical properties, the formation of supersaturated solid solutions is desired, which can be achieved via nonequilibrium processes such as melt spinning [127,128] and physical vapor deposition [49,93]. Take aluminum–manganese alloys as an example, manganese (Mn) has very limited solubility in aluminum from the binary phase diagrams. Under low temperatures, the equilibrium solubility of manganese in aluminum is less than 0.1 percent. So, this first strategy forms a supersaturated solid solution, taking advantage of non-equilibrium processing methods such as physical vapor deposition so that the material can be strengthened to improve its wear resistance without the deformation of secondary phase.

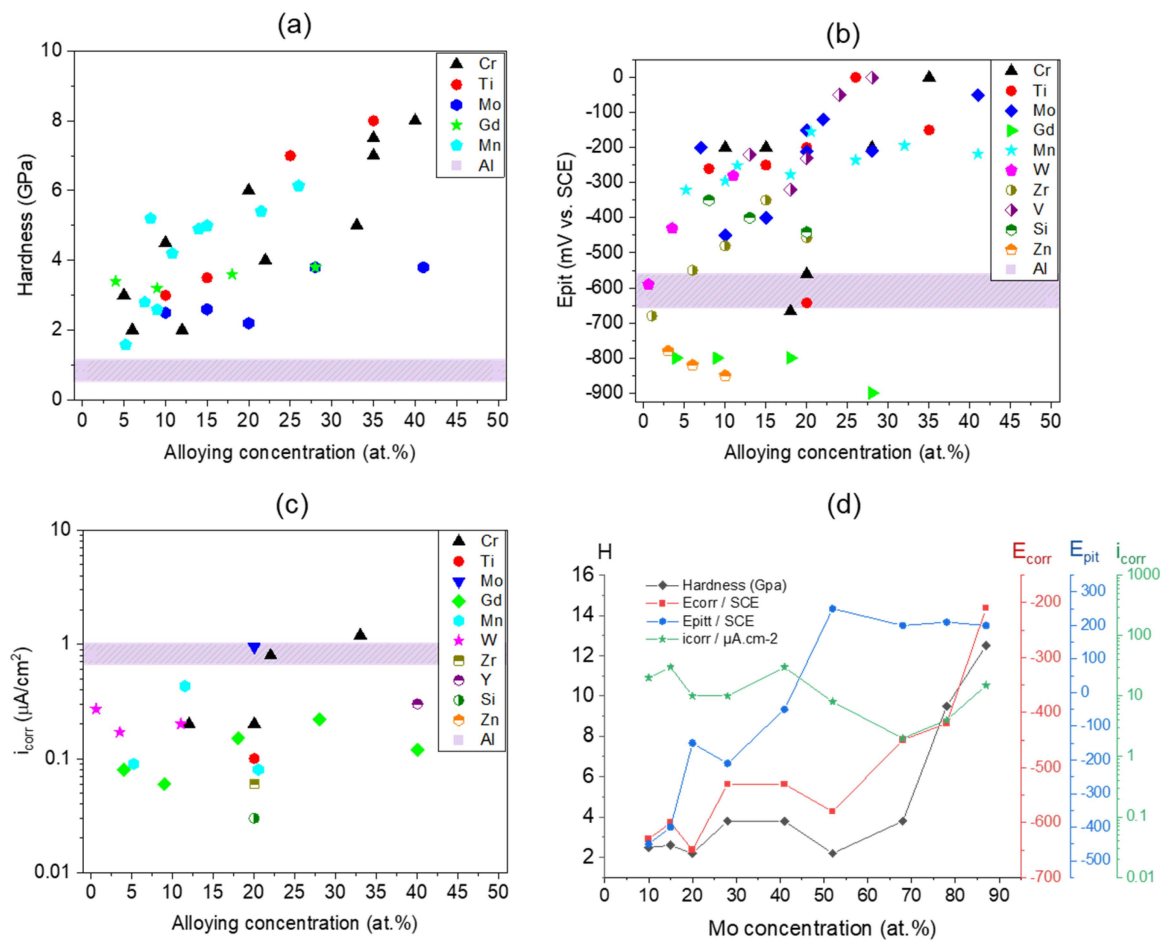


**Figure 7.** Summary of (a) Hardness (H); (b) Pitting potential ( $E_{pit}$ ); and (c) Corrosion current density ( $i_{corr}$ ) as a function of alloying concentration in binary Al–X systems [93,118,129–136] (replotted from Ref. [49]). (d) Dependence of hardness (H), corrosion potential ( $E_{corr}$ ), pitting potential ( $E_{pit}$ ), and corrosion current ( $i_{corr}$ ) as a function of Mo concentration in Al–Mo binary alloy (plotted using data from [134]).

### 7.1.1. Alloying Effects on Corrosion

Using such a strategy, Maried et al. [49,93] studied the effects of Mn concentration on the corrosion behavior of Al–Mn solid solutions prepared via physical vapor deposition (Figure 8a). The addition of Mn was found to significantly enhance the corrosion resistance of Al (Figure 8a). The pitting potential showed a consistent increase with increasing Mn concentration and remained unaffected by the microstructure, provided chemical homogeneity was achieved (Figure 8b).

Notably, the alloys with fully nanocrystalline (5.2 at.% Mn) and fully amorphous (20.5 at.% Mn) microstructures displayed superior corrosion resistance compared to those with a dual-phase microstructure (11.5 at.% Mn). Later on, Jia et al. [137] investigated the influence of Mn on the aqueous corrosion of Al–Mn alloys through experiments and atomistic simulations. Interestingly, electrochemical measurements, X-ray photoelectron spectroscopy, and atom probe tomography analysis revealed that the addition of Mn improved the corrosion resistance of Al without actively participating in surface oxidation (Figure 9a,b).

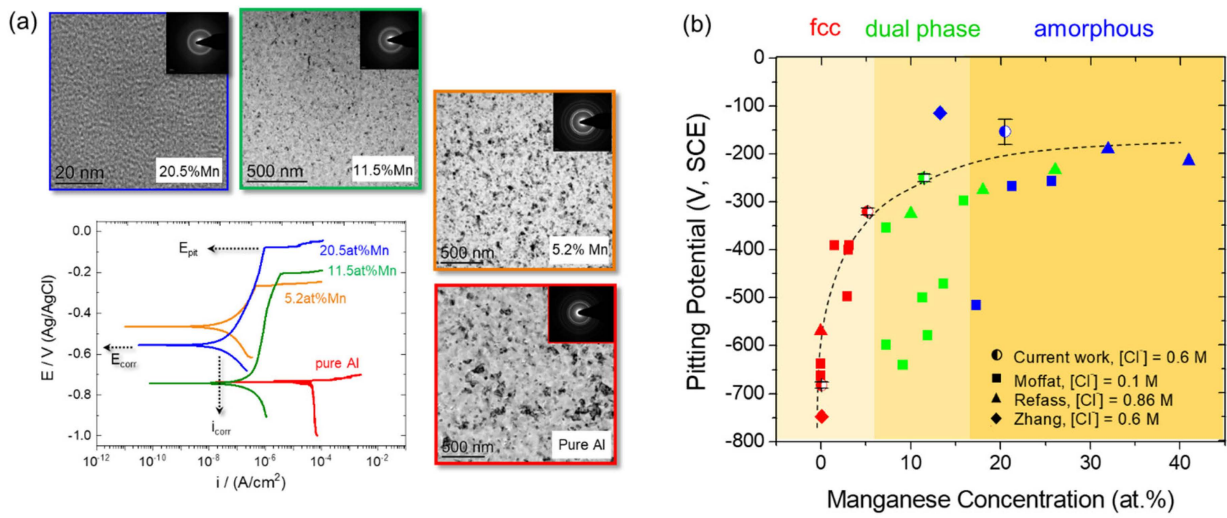


**Figure 8.** Summary of microstructure corrosion behavior of Al-Mn supersaturated solid solutions in 0.6 M NaCl electrolyte. (a) Potentiodynamic polarization curves and their corresponding transmission electron microscopy images of pure Al, Al-5.2 at.% Mn, Al-11.5 at.% Mn, and Al-20.5 at.% Mn. (b) Relationship between pitting potential and manganese concentration with different phases. Replotted from Refs. [49,93].

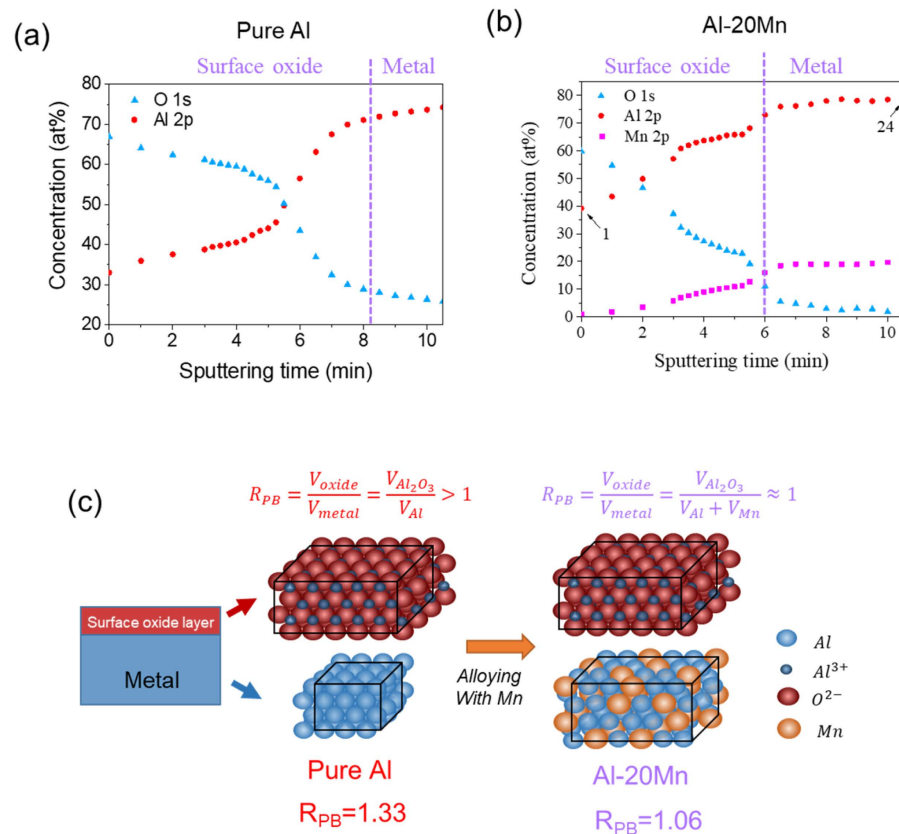


**Figure 9.** (a) Corrosion current and (b) Corrosion potential of Al-Mn solid solutions with 0–40 at.% Mn. (c) Schematic summary of how Mn addition influences the passive layer protectiveness. Replotted from Ref. [137].

A mechanism explaining the roles of Mn on the protectiveness of the passive layer of Al is shown in Figure 9c. It was suggested that selective dissolution of Mn increased the available free volume at the metal/oxide interface, leading to the formation of a denser

and thinner oxide layer with a composition closer to stoichiometry. Additional molecular dynamics simulations supported these findings, demonstrating that an increase in free volume content in Al resulted in a more compact oxide layer with reduced defect density, ultimately contributing to enhanced barrier characteristics. Quantitatively, this model takes into account an effective Pilling–Bedworth (PB) ratio,  $R_{PB}$ , and of the binary alloy, which has significant implications for the structural compatibility between the metal and oxide. Optimizing the alloy composition to achieve an effective  $R_{PB}$  close to one result in the formation of a highly protective naturally occurring oxide layer. For the three alloys: pure Al, Al-1.6 at.% Mn, and Al-20 at.% Mn, the effective  $R_{PB}$  value is 1.33, 1.31, and 1.06, respectively, supporting such hypotheses. Interestingly, this simple model also provides an explanation for the observed decrease in the pitting potential of Al–Mn alloys when Mn% exceeds around 40 at.% [138], resulting in an  $R_{PB}$  value of 0.8, significantly lower than 1. As a consequence, the formed oxide layer lacks sufficient volume to completely cover the metal substrate for effective passivation. Using such a model, Chen et al. [139] designed highly corrosion-resistant Al–Mn–Mo alloys with optimum alloying concentrations of Mn and Mo.

#### 7.1.2. Alloying Effects on Tribocorrosion and Wear-Corrosion Synergy

In terms of tribocorrosion, Mraied and Cai [49] showed that alloying Al with Mn supersaturated solid solutions simultaneously enhanced the wear resistance and protective properties of the passive layer, resulting in improved overall tribocorrosion resistance. Higher Mn content increased the hardness-to-elastic modulus ratio (H/E) and promoted the formation of a denser and more compact passive film, thereby enhancing the tribocorrosion resistance of Al. Alloying with 20.5 at.% Mn, in particular, led to approximately 10 times higher corrosion resistance and 8 times greater hardness compared to pure Al. The total material loss during tribocorrosion was observed to increase with the anodic shift of the applied potential. It was found that alloying with 5.2 at.% Mn resulted in more than a 10-fold reduction in the current density required to re-passivate similar worn areas of pure Al.

In terms of wear-corrosion synergy (S), the behavior of both corrosion-accelerated wear and wear-accelerated corrosion were measured (Figure 10). For the former, the total material loss during tribocorrosion of Al–Mn was observed to rise with the applied potential (Figure 10c). At cathodic potentials, tribocorrosion is dominated by mechanical wear, and the overall material loss is primarily influenced by the mechanical properties of the material. However, under open circuit and anodic potentials, mechanical wear causes local depassivation of the wear track, leading to active corrosion and accelerated material loss. For wear-accelerated corrosion, the rise of corrosion current during scratching is a clear indication (Figure 10d).

Such a current rise was found to be reduced at higher Mn concentrations. It should also be pointed out that the relative fraction of pure wear, pure corrosion, and wear-corrosion synergy in the total material loss (Figure 10b) depends not only on the material property (e.g., alloying concentration and grain size), but also on the testing condition, such as the sliding frequency. For example, Chen and Cai [62] showed that as the frequency increased, both chemical and mechanical wear increased (Figure 11a). The rise in mechanical wear with frequency was attributed to a faster depassivation rate and an increase in the real contact area. The schematic summary of how Mn addition influences the passive layer protectiveness is shown in Figure 11b.

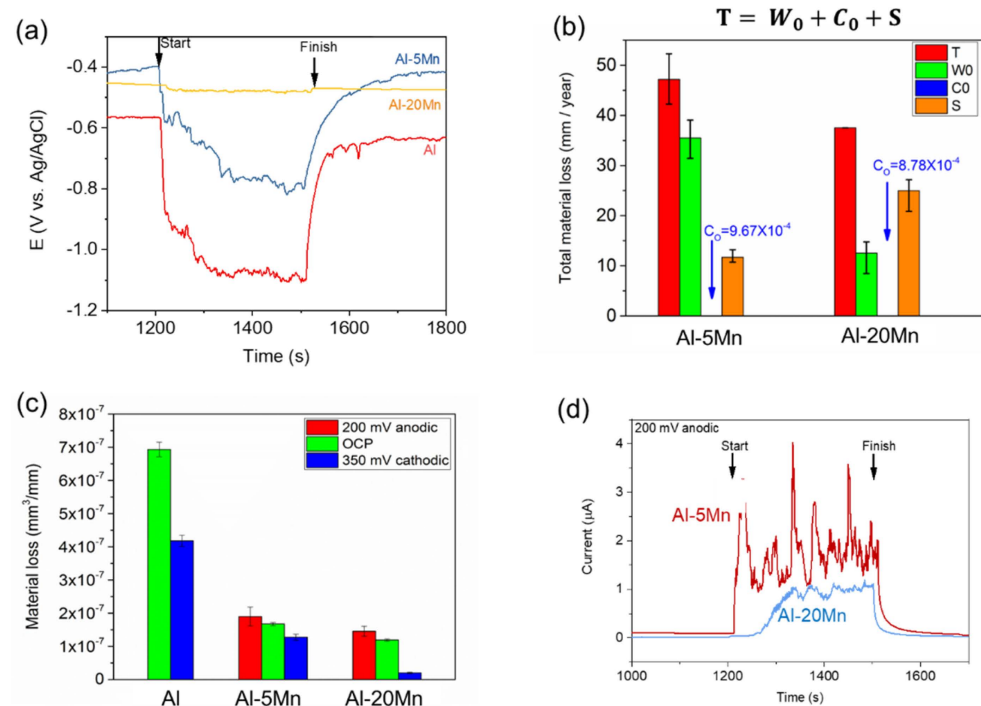


**Figure 10.** (a) Evolution of open circuit potential; (b) Summary of material loss from wear, corrosion, and synergy; (c) Material loss as a function of applied potential; and (d) Temporal evolution of tribocorrosion current at 200 mV anodic potential of Al and Al–Mn alloys after tribocorrosion tests in 3.5 wt.% NaCl solutions. Replotted from Refs. [49,93].

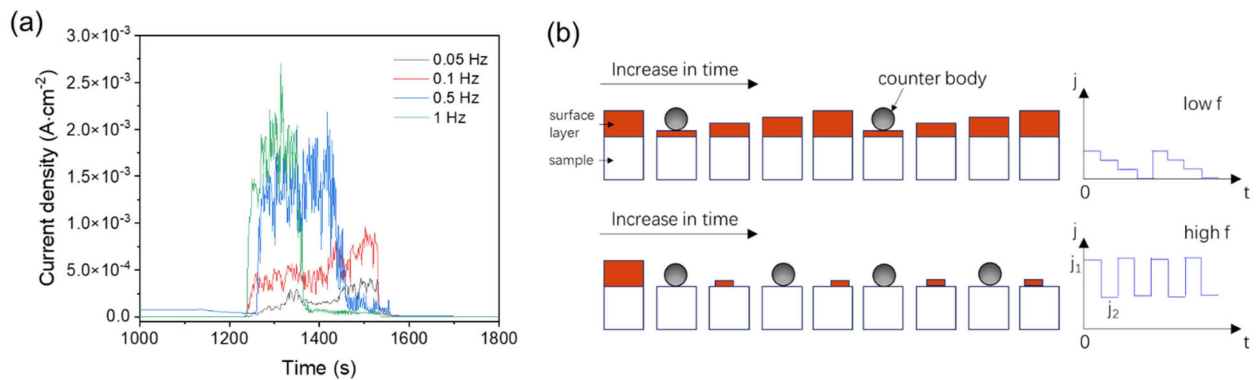


**Figure 11.** (a) Corrosion current of Al–Mn solid solutions with 0–40 at.% Mn. (b) Schematic summary of how Mn addition influences the passive layer protectiveness. Replotted from Ref. [62].

However, the increase in chemical wear with frequency was linked to higher repassivation kinetics. Similar to the pure corrosion condition, the outermost surface layer was found to be rich in aluminum and oxygen but lacking in manganese. In conclusion, the addition of supersaturated solution solid offers great opportunity to simultaneously enhance wear and corrosion resistance, ultimately achieving our design goal, as shown in Figure 12. The effective Pilling–Bedworth ratio can be used as a guideline to tailor the optimum alloying concentration of complex systems.

### 7.2. Strategy 2: Formation of Nanostructured Multilayers

Motivated by the grain size effect, the second strategy involves creating a nanostructured layered structure for enhancing tribocorrosion resistance. Such nanolayering can be synthesized via physical or chemical vapor deposition [140], or form as a result of severe plastic deformation [81]. Nanostructured metallic multilayers (NMMs) have garnered

significant attention due to their potential to enhance both mechanical and electrochemical properties when compared to monolithic materials [141]. Our recent study [142] demonstrated that NMMs exhibit remarkably high tribocorrosion resistance due to their abundant interfaces and nanoscale chemical modulation, which effectively limits plastic deformation and reduces micro-galvanic corrosion and surface reactivity. Specifically, the tribocorrosion behavior of NMMs composed of equal-spaced Al/X (X = Ti, Mg, and Cu) layers, each with a thickness of approximately 3 nm was investigated in a 0.6 M NaCl aqueous solution at room temperature (Figure 13).

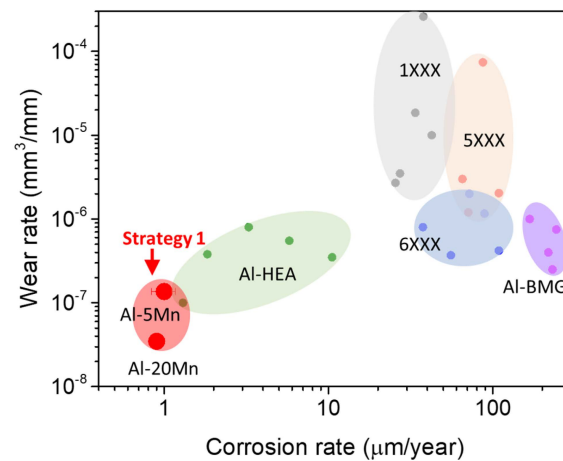


**Figure 12.** Summary of wear rate versus corrosion of Al-based alloys from literature review. Strategy 1 indicates the formation of supersaturated solid solution. Plotted using data obtained from Refs. [49,93,124,125]. Al-HEA represents  $\text{Al}_x\text{Co}_{1.5}\text{CrFeNi}_{1.5}\text{Ti}_y$  high-entropy alloys, Al-BMG represents  $\text{Al}_{90.05}\text{Y}_{4.4}\text{Ni}_{4.3}\text{Co}_{0.9}\text{Sc}_{0.35}$  bulk metallic glasses, and 1xxx, 5xxx, and 6xxx represents different-series of Al alloys.

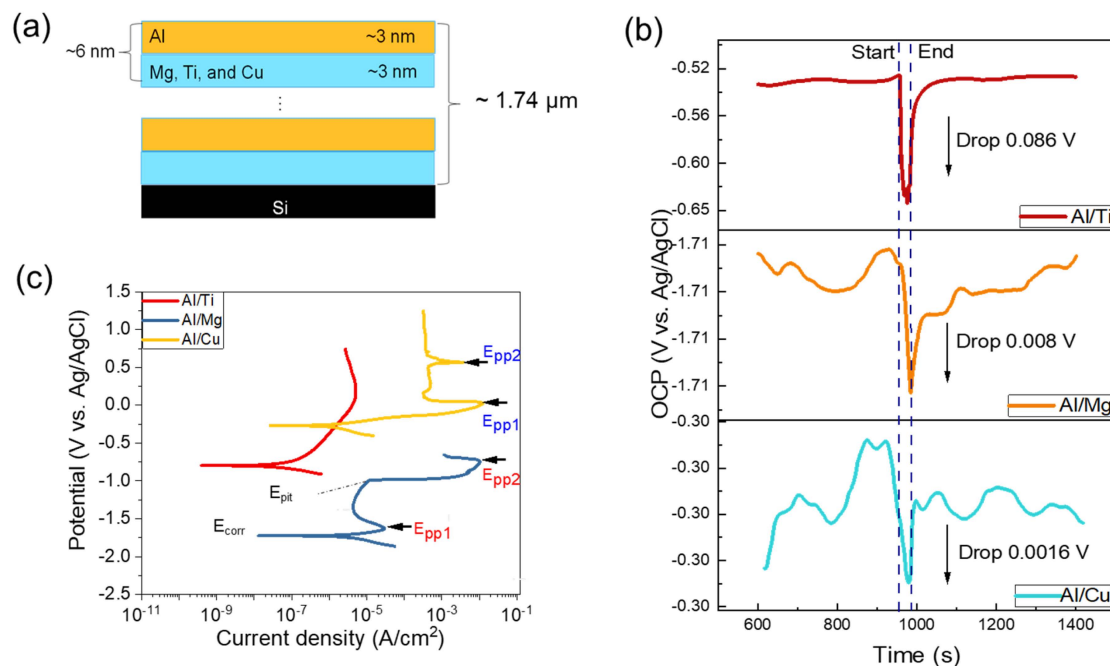


**Figure 13.** (a) Schematic of Al/X NMM structure; (b) Evolution of open circuit potential (OCP) during tribocorrosion; and (c) Potentiodynamic polarization curves of Al/X (X = Ti, Mg, and Cu) in 3.5 wt.% NaCl. Replotted from Ref. [142].

It was found that corrosion dominated in the tribocorrosion behavior of Al/Mg and Al/Cu NMMs, while severe plastic deformation prevailed in Al/Ti NMMs due to sustained surface passivity. In addition to experimental measurements, a finite element (FE) based computational model was developed and validated to understand the tribocorrosion mechanisms of NMMs. This model showed accelerated material loss at layer interfaces and wear track edges, resulting from the synergistic effects of wear and corrosion (Figure 14).

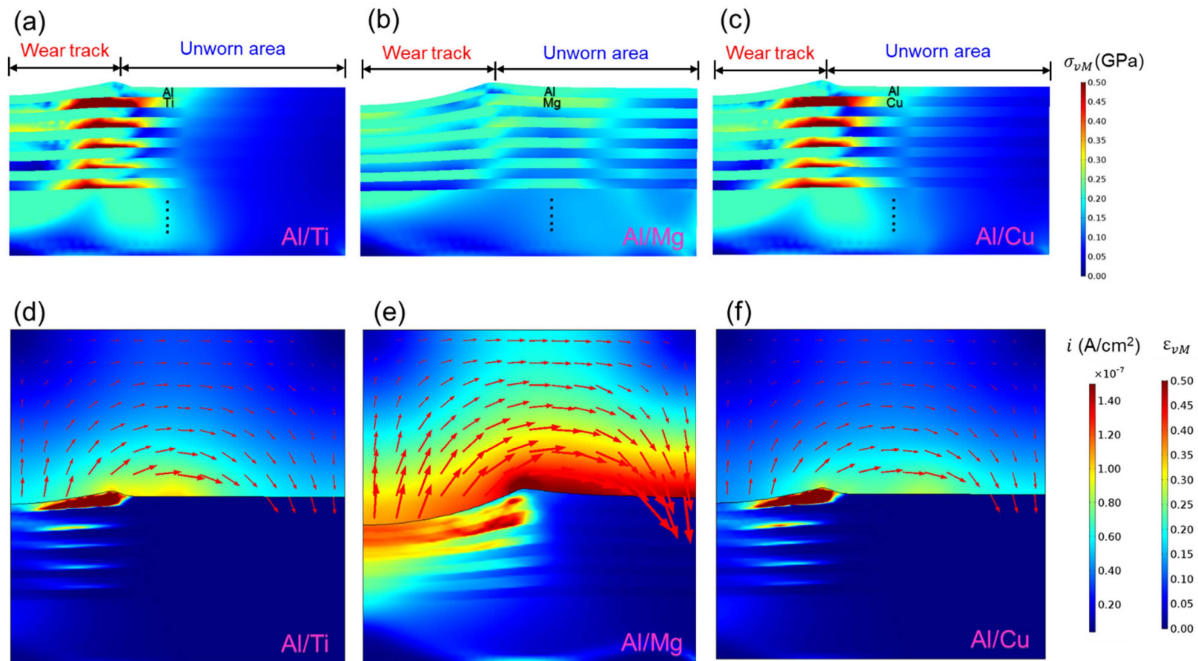


**Figure 14.** Finite element (FE) simulation results of (a–c) von Mises stress distribution after wear; and (d–f) von Mises strain and current density distribution after tribocorrosion in 0.6 M NaCl aqueous solution of Al/Ti, Al/Mg, and Al-Cu NMMs. Replotted from Ref. [142].

To understand the structural origin of the enhanced tribocorrosion resistance, density functional theory (DFT) calculations were conducted to uncover the surface property of NMMs [142]. It was observed that nanolayering with Ti increased the surface work function of Al while reducing the adsorption strength of Cl adatoms compared to pure Al, thereby lowering the surface reactivity and susceptibility to pitting. Later on, using multiphysics finite element modeling, Wang and Cai [143] showed that in Al–Cu NMMs, thinner individual layers in the corrosion process result in a more concentrated current exchange between these layers. As a result, this enhances the cathodic protection of copper (Cu) layers and promotes the formation of a passive layer on exposed aluminum (Al) layers, ultimately enhancing the tribocorrosion resistance. This model also reveals that the layer orientation significantly influences the overall tribocorrosion behavior of NMMs. In NMMs with vertical layers, deeper material loss was observed in the softer Al layers, resulting in higher volume loss from both wear and corrosion processes. On the contrary, in NMMs with parallel layers, the Cu layers act as a barrier, impeding material removal and helping to maintain the integrity of the layers below. This also reduces the exposure of depassivated Al surface area, leading to less severe anodic corrosion of the Al layers and a faster repassivation process. Consequently, the vertically aligned multilayers are more susceptible to the threats of tribocorrosion compared to the horizontally aligned multilayers. In conclusion, the second strategy of nano layering offers great opportunity to simultaneously enhance wear and corrosion resistance. As shown in Figure 15, the hardness, corrosion rate (Figure 15a), and tribocorrosion performance (Figure 15b) of NMMs are all enhanced compared to their monolithic counterparts and commercial Al alloys.

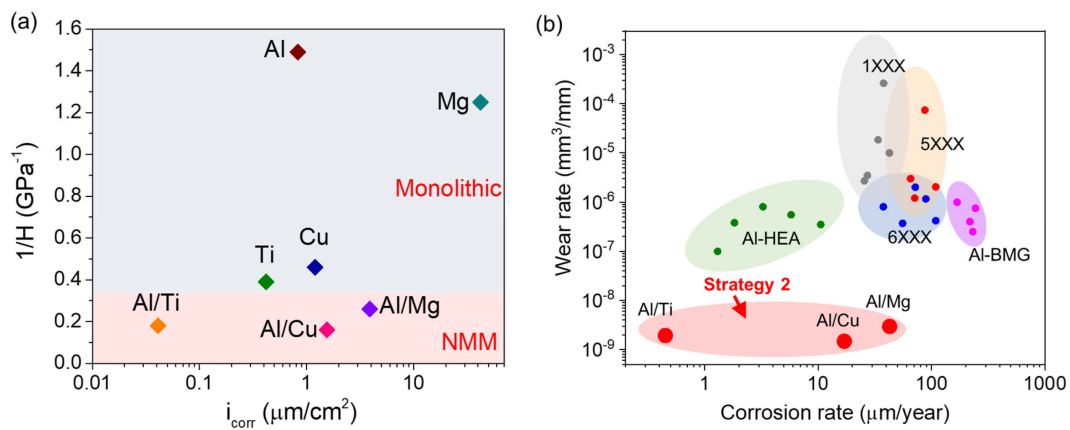


**Figure 15.** Summary of (a)  $1/H$  vs.  $i_{\text{corr}}$  of all monolithic and NMM samples; and (b) wear versus corrosion rate of all samples in the present work, as well as 1xxx, 5xxx, and 6xxx Al alloys, Al-based high entropy alloys (HEA), and Al-based bulk metallic glasses (BMG) tested under similar conditions.

### 7.3. Strategy 3: Formation of Preferred Crystallographic Textures

The last alloy design strategy involves optimizing the preferred crystallographic orientations, i.e., texture of alloys to simultaneously minimize wear and corrosion. Texture has been known to affect the tribological response of metals [67]. Similar strategies have been applied in tailoring the mechanical [144] and corrosion properties of fcc and hcp metals such as Ti6Al4V [123,145] alloys and additively manufactured parts [146]. In terms of Al, recently, Wang et al. [147] performed a combined experimental and computational investigation using Al (100), (110), and (111) single crystals to establish a crystal-based tribocorrosion modeling framework that considers the influence of lattice reorientation and dislocations on surface corrosion (see model schematic in Figure 16).

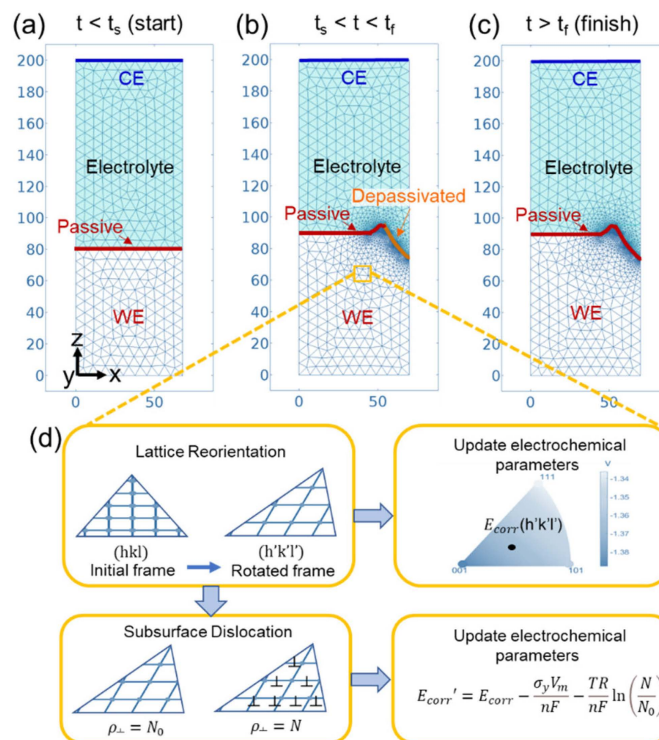


**Figure 16.** Summary of the FE tribocorrosion model setup and geometry (a) Before; (b) During; and (c) After the tribocorrosion test. (d) Schematic of the local electrochemical parameter mapping as a function of the lattice reorientation and dislocation density. Replotted from Ref. [147].

Specifically, the mechanical, corrosion, and tribocorrosion properties of Al single crystals were measured to be highly anisotropic, depending on the crystal orientation (Figure 17). Among all three orientations, the wear resistance and corrosion resistance of the (100) Al sample is the worst and (111) is the best. With the experimental results as inputs and validation, a multiphysics finite element model was developed. This model successfully predicted the depassivation and repassivation currents during the tribocorrosion of Al single crystals by mapping the local corrosion kinetics based on the passivation state, crystallographic orientation, and dislocation density (Figure 17c,d). The study revealed that lattice rotation, rather than dislocations, played a dominant role in the overall tribocorrosion behavior. This work uses single crystals as model materials, which paves the way for future modeling of the tribocorrosion behavior polycrystalline materials with random or preferred texture.

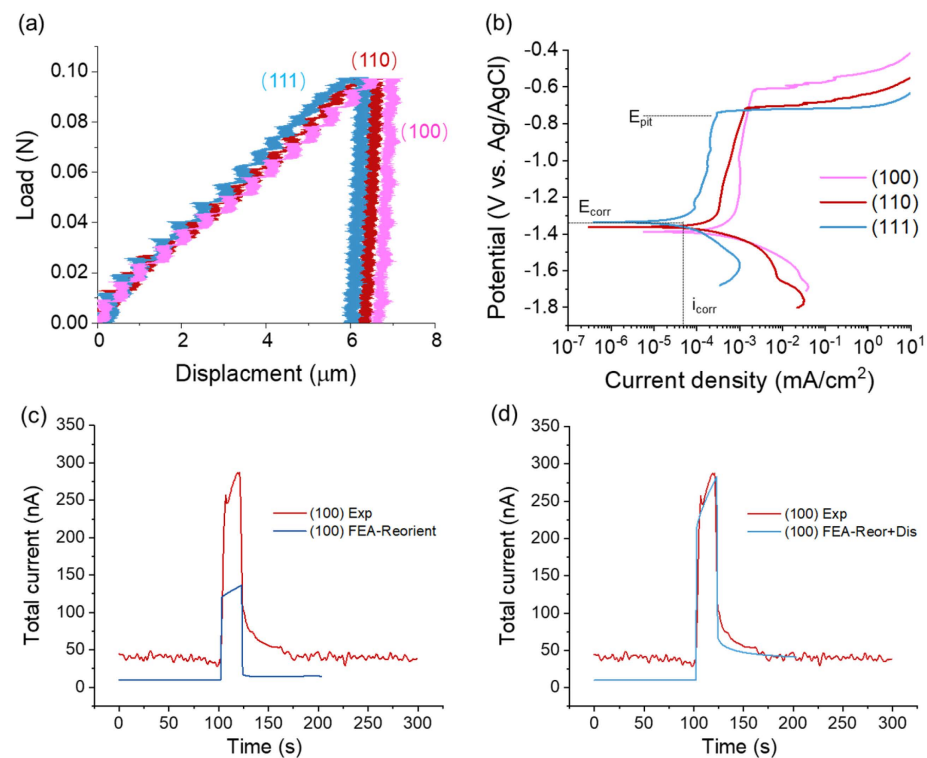


**Figure 17.** (a) Nanoindentation results and (b) Potentiodynamic polarization curves of Al (100), (110), and (111) single crystals in 3.5 wt.% NaCl solution. Tribocorrosion current evolution of experimentally measured profiles v.s. finite element analysis simulated profiles (c) Without and (d) With consideration of subsurface dislocation effects. Replotted from Ref. [147].

## 8. Current Challenges and Outlook

While this field has made significant advancements in understanding the interactions between tribology and corrosion, it still faces several challenges that researchers are actively working to overcome. Here are some of the current challenges and opportunities in tribocorrosion study:

**Material Characterization:** Accurate characterization of material properties, especially at the surface, is crucial in tribocorrosion studies. The complex coupling between wear-induced dislocation activities and corrosion-induced surface oxidation or dissolution makes the surface and subsurface structure and composition of the tribocorroded surfaces far away from those of the bulk. Obtaining reliable data on surface composition, defect structure, oxide/metal interface properties can be challenging, limiting the accuracy of predictive models. Great opportunities exist in utilizing and developing advanced microscopy and spectroscopy to characterize the surface materials as a result of interactions with corrosive

environments [148]. A better understanding of such far-from-equilibrium surfaces should be very helpful for designing future tribocorrosion-resistant metals.

**Multi-Scale and Multi-Physics Nature:** The mechanisms governing tribocorrosion processes are still not fully understood due to their complexity. There is a need to delve deeper into the fundamental interactions between wear, corrosion, and the synergistic effects that occur at the material interfaces. On one hand, the tribocorrosion behavior of materials is highly influenced by environmental factors such as temperature, humidity, and pH. Understanding how these variables affect the tribocorrosion processes is essential for practical applications. However, tribocorrosion phenomena occur at multiple length and time scales, ranging from atomic interactions at the material/environment interface to macroscopic wear and corrosion kinetics. Bridging these scales to develop comprehensive models that accurately predict material behavior remains a challenge. Thirdly, wear and corrosion are not independent from each other. The wear-corrosion synergy can significantly affect material degradation. However, the precise conditions and factors that govern this synergy are not fully understood, making it difficult to predict material behavior accurately.

**Material Selection and Design:** Designing materials with enhanced resistance to tribocorrosion is a challenge due to the trade-off between wear and corrosion resistance in most metallic materials. Besides the three alloy design strategies discussed earlier, there is a need to explore electrochemically benign strengthening mechanisms. That is, one that would strengthen the material without compromising (and if possible, even improving) the corrosion resistance [149,150]. One such opportunity lies in grain boundary engineering, which has been found to improve both wear and intergranular stress corrosion cracking resistance [151,152]. Advanced surface manufacturing such as laser shock peening also offer great promise to optimize surface properties including corrosion and tribocorrosion resistance [153]. Finally, material selection is challenging due to the difference in the target environment [154]. For example, a tribocorrosion-resistant metal for seawater might not be the best choice for an acidic solution or body fluids. A holistic view is required when considering material selection for specific practical applications. Some of the new emerging technologies might require new alloy development to meet the structural integrity requirements in some very unusual environments, such as deep sea, outer space, and molten salt.

Looking into the future, the synergistic use of experimental, computational, and modeling techniques, along with the incorporation of advanced tools like machine learning and multiphysics simulations, holds the potential to unravel complex interactions and pave the way for innovative solutions in materials engineering and tribocorrosion mitigation [155,156]. Towards this end, one promising avenue for future research lies in the development of multiphysics modeling approaches, particularly the creation of tribocorrosion rate maps. An example is shown in Figure 18, based on recent work by Wang et al. [157]. These maps combine information from multiple physical processes, such as mechanical wear, corrosion kinetics, and electrochemical interactions to provide a comprehensive understanding of tribocorrosion behavior as a function of both mechanical and electrochemical parameters. Such maps can be invaluable in guiding material selection, engineering designs, and maintenance planning for systems prone to tribocorrosion, leading to more durable and reliable performance in corrosive environments.

Another future direction involves the incorporation of data science and machine-learning techniques [158]. Machine learning has shown tremendous potential in various fields, including wear and corrosion studies. By harnessing the power of machine-learning algorithms, researchers can analyze vast amounts of data from experimental and computational sources to identify patterns, correlations, and hidden insights. This can aid in predicting wear and corrosion behavior, optimizing material design, and developing proactive strategies for mitigating tribocorrosion effects [144]. For example, recently, Lee et al. [159] developed an active learning model to enhance the efficiency of data collection in tribocorrosion systems that are expensive to evaluate. By employing active learning in

conjunction with surrogate modeling, it becomes feasible to analyze demanding tribocorrosion systems in a cost-effective manner by partitioning the material property design space (which include both mechanical and electrochemical properties) based on heterogeneous features such as volume loss due to wear and corrosion. The informativeness of new design points is quantified while mitigating the system heterogeneity. This partitioning enables two systematic steps in the search for the next design point (i.e., optimum material properties). A global searching scheme expedites exploration by identifying the most uncertain subregion. Subsequently, a local searching approach leverages the localized Gaussian process (GP) information to make more informed decisions. The efficacy of this integrated data science and machine-learning method is found to outperform existing active learning methods and traditional finite element modeling, showcasing superior predictive accuracy and reduced computation time.

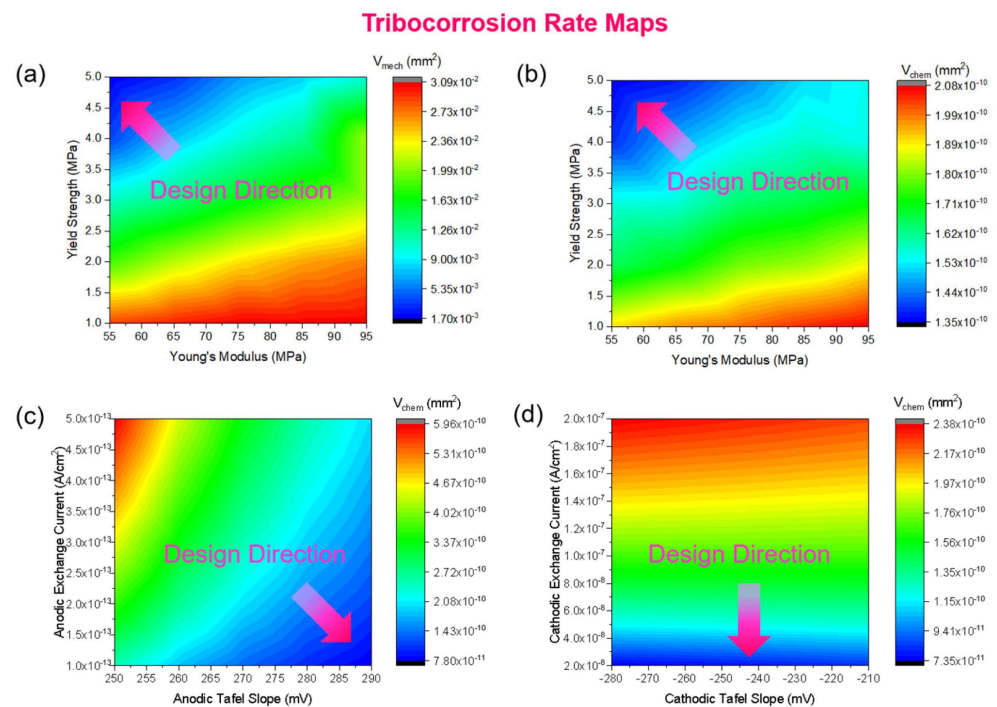


**Figure 18.** Summary of tribocorrosion rate maps predicted via multiphysics modeling. Material volume loss (a) from mechanical wear and (b–d) chemical wear as a function of (a,b) yield strength and Young's modulus, and (c,d) electrochemical properties of Al-based alloys. Replotted from Ref. [157].

In the future, new alloy systems and unique microstructure engineering offer great promise to further enhance tribocorrosion resistance. Towards this end, the development of both dilute and concentrated Al-based alloys (e.g., high entropy alloy and metallic glasses) are worth further studies. For dilute Al-based alloys, several alloy systems have been reported with good mechanical and corrosion properties, such as Al–Mg–Bi [160], Al–Ce–X (X = Sc, Y, etc.) [161–163], and Al–Mg–Sc-based alloys such as Scalmalloy [164,165]. For Al-based concentrated alloys, Al<sub>0.7</sub>FeCoCrNiCu<sub>x</sub> HEAs [166] and AlNiZr amorphous alloys [167] are found to be outstanding corrosion- and wear-resistant structural materials in salty environments.

In terms of microstructure engineering, those that favor electrochemically benign strengthening mechanisms are also worth exploring, which will likely strengthen the material and increase the hardness without compromising the corrosion resistance. For example, recently, Jia et al. [168] showed that deep cryogenic treatment (DCT) provides a driving force for nucleation and growth during the re-aging treatment of the AA2024 alloy. The combined aging and DCT treatment significantly improve the wear resistance of

AA2024 without affecting the corrosion resistance, which is likely to enhance the overall tribocorrosion resistance. Compositionally and/or microstructurally gradient surfaces is another promising route of microstructure engineering that is worth looking into towards enhanced tribocorrosion resistance. Such gradient structured materials can be synthesized via additive manufacturing [169] or surface treatment such as ultrasonic impact treatment (UIT) [170], laser-shock peening (LSP) [153], and surface-mechanical attrition (SMAT) [170, 171]. For example, Dai et al. [169] showed that the grain size gradient from  $\sim 5 \mu\text{m}$  equiaxed grains to  $38 \mu\text{m}$  columnar grains can be obtained at the surface of 2319 aluminum alloy via a hybrid wire-arc additive manufacturing (WAAM) and friction stir processing (FSP) additive manufacturing technology. Beura et al. [172] investigated the corrosion behavior of SMAT-processed aluminum 7075 alloy and found reduced anodic dissolution rate due to the surface microstructural changes such as the formation of precipitates and dissolution of inherent phases imposed by SMAT. In addition, a reduced anodic was observed with the SMAT processed samples.

Finally, the tribocorrosion behavior of Al alloys in other extreme environment remains largely unexplored, such as deep ocean [64], hydrogen-containing environments, hydrostatic pressure [173], high-temperature oxidatives [174], and mining environments [175]. The exploration of stressed corrosion and tribocorrosion of Al alloys under such environments opens new possibilities for the development of a variety of future technologies. For example, David et al. [173] found that lightweight and corrosion-resistant aluminum nanocomposites are promising candidates for in-pipe robots for sewage cleaning purposes, which also allows for detection of pipeline leakage, crack, gas, and corrosion detection.

## 9. Summary

In summary, tribocorrosion represents an emerging field with significant implications both in fundamental research and practical applications. This paper reviews the current understanding on the alloying and grain size effects on tribocorrosion and summarizes three alloy design strategies to combat the wear-corrosion resistance tradeoff, as shown in Figure 19.

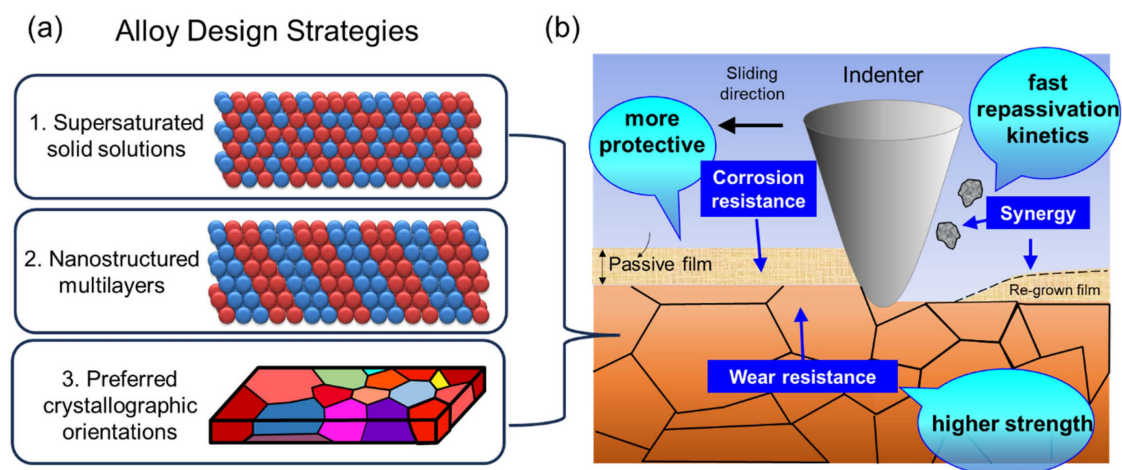


**Figure 19.** Summary of (a) Three alloy design strategies and (b) Relevant tribocorrosion mechanism of metals due to the alloy design.

Strategy 1 involves forming supersaturated solid solutions to simultaneously strengthen the material and enhance the corrosion resistance and repassivation kinetics. Strategy 2 tailors tribocorrosion behavior by optimizing a structural length scale of chemical modulation, i.e., the individual layer thickness of nanostructured metallic multilayers and superlattices. When such length scale is controlled at a few nanometers, simultaneous high wear and corrosion resistance can be obtained, especially if all alternative layers are composed of passive metals such as Al and Ti. Strategy 3 is more applicable to general polycrystalline

materials, where preferred crystallographic orientation, i.e., texture, can be controlled by manufacturing to optimize tribocorrosion behavior. For Al, among various low index (i.e., high symmetry) planes, the wear resistance and corrosion resistance of the (100) orientation is the worst and (111) is the best.

We conclude by addressing several current challenges and suggesting a few promising future research directions in the field of tribocorrosion. In the future, the integration of experimental, computational, and modeling techniques, coupled with advanced tools like machine learning and multiphysics simulations, offers the potential for innovative solutions in materials engineering and tribocorrosion mitigation. The potential for improved tribocorrosion resistance also lies in the development of new alloy systems and microstructure engineering techniques. This includes the exploration of both dilute and concentrated Al-based alloys. Novel microstructure designs that enhance the material's strength and hardness through electrochemically benign mechanisms while preserving corrosion resistance is valuable. Finally, the tribocorrosion behavior of Al alloys in extreme environments like the deep ocean, hydrogen-containing atmospheres, hydrostatic pressure, high-temperature oxidative conditions, and mining environments remains largely uncharted territory. Exploring the corrosion and tribocorrosion of Al alloys in such contexts has the potential to drive innovations in various future technologies.

**Funding:** The authors gratefully acknowledge funding provided by US National Science Foundation (DMR-1856196, CMMI-1855651 and DMR-2104655).

**Data Availability Statement:** Data available on proper request from the authors.

**Conflicts of Interest:** The authors declare no conflict of interest.

## References

1. ASTM G40-10b; Standard Terminology Relating to Wear and Erosion. ASTM International: West Conshohocken, PA, USA, 2010.
2. Landolt, D.; Mischler, S. *Tribocorrosion of Passive Metals and Coatings*; Woodhead Publishing Series in Metals and Surface Engineering; EPFL: Lausanne, Switzerland, 2011.
3. Mischler, S. Sliding Tribo-Corrosion of Passive Metals: Mechanisms and Modeling. In *Tribo-Corrosion: Research, Testing, and Applications*; Peter, J.-P., Blau, J., Celis, D.D., Eds.; ASTM International: Atlanta, GA, USA, 2013; pp. 1–18.
4. Landolt, D.; Mischler, S.; Stemp, M. Electrochemical methods in tribocorrosion: A critical appraisal. *Electrochim. Acta* **2001**, *46*, 3913–3929. [[CrossRef](#)]
5. Panțuru, M.; Chicet, D.; Paulin, C.; Alexandru, A.; Munteanu, C. Wear aspects of internal combustion engine valves. *IOP Conf. Ser. Mater. Sci. Eng.* **2016**, *147*, 012036. [[CrossRef](#)]
6. Macdonald, D.D. Passivity—The key to our metals-based civilization. *Pure Appl. Chem.* **1999**, *71*, 951–978. [[CrossRef](#)]
7. Wolf, D.; Yamakov, V.; Phillpot, S.R.; Mukherjee, A.; Gleiter, H. Deformation of nanocrystalline materials by molecular-dynamics simulation: Relationship to experiments? *Acta Mater.* **2005**, *53*, 1–40. [[CrossRef](#)]
8. Rupert, T.J.; Schuh, C.A. Sliding wear of nanocrystalline Ni-W: Structural evolution and the apparent breakdown of Archard scaling. *Acta Mater.* **2010**, *58*, 4137–4148. [[CrossRef](#)]
9. Pokhmurs'kyi, V.I.; Dovhunyuk, V.M. Tribocorrosion of Stainless Steels (Review). *Mater. Sci.* **2010**, *46*, 87–96. [[CrossRef](#)]
10. Wood, R.J. Tribo-corrosion of coatings: A review. *J. Phys. D Appl. Phys.* **2007**, *40*, 5502–5521. [[CrossRef](#)]
11. García-León, R.A.; Afanador-García, N.; Guerrero-Gómez, G. A Scientometric Review on Tribocorrosion in Hard Coatings. *J. Bio-Tribo-Corros.* **2023**, *9*, 39. [[CrossRef](#)]
12. Kolawole, F.O.; Kolade, O.S.; Bello, S.A.; Kolawole, S.K.; Ayeni, A.T.; Elijah, T.F.; Borisade, S.G.; Tschiptschin, A.P. The improvement of diamond-like carbon coatings for tribological and tribo-corrosion applications in automobile engines: An updated review study. *Int. J. Adv. Manuf. Technol.* **2023**, *126*, 2295–2322. [[CrossRef](#)]
13. Mischler, S.; Rosset, E.; Stachowiak, G.W.; Landolt, D. Effect of sulphuric acid concentration on the rate of tribocorrosion of iron. *Wear* **1993**, *167*, 101–108. [[CrossRef](#)]
14. Landolt, D. Electrochemical and materials aspects of tribocorrosion systems. *J. Phys. D Appl. Phys.* **2006**, *39*, 3121. [[CrossRef](#)]
15. López-Ortega, A.; Arana, J.L.; Bayón, R. Tribocorrosion of Passive Materials: A Review on Test Procedures and Standards. *Int. J. Corros.* **2018**, *2018*, 7345346. [[CrossRef](#)]
16. ASTM G119-09; Standard Guide for Determining Synergism between Wear and Corrosion. ASTM International: West Conshohocken, PA, USA, 2016.
17. UNE 112086:2016; Ensayos de Tribocorrosión en Materiales Pasivos. UNE: Madrid, Spain, 2016.
18. Maher, M.; Iraola-Arregui, I.; Ben Youcef, H.; Rhouta, B.; Trabadelo, V. The synergistic effect of wear-corrosion in stainless steels: A review. *Mater. Today Proc.* **2022**, *51*, 1975–1990. [[CrossRef](#)]

19. Apaza-Bedoya, K.; Tarce, M.; Benfatti, C.A.M.; Henriques, B.; Mathew, M.T.; Teughels, W.; Souza, J.C.M. Synergistic interactions between corrosion and wear at titanium-based dental implant connections: A scoping review. *J. Periodontal Res.* **2017**, *52*, 946–954. [[CrossRef](#)] [[PubMed](#)]
20. Abolusoro, O.P.; Akinlabi, E.T. Tribocorrosion Measurements and Behaviour in Aluminium Alloys: An Overview. *J. Bio-Tribo-Corros.* **2020**, *6*, 102. [[CrossRef](#)]
21. Igual Munoz, A.; Espallargas, N.; Mischler, S. Tribocorrosion: Definitions and Relevance. In *Tribocorrosion*; Igual Munoz, A., Espallargas, N., Mischler, S., Eds.; Springer International Publishing: Cham, Switzerland, 2020; pp. 1–6. [[CrossRef](#)]
22. Mischler, S.; Debaud, S.; Landolt, D. Wear-Accelerated Corrosion of Passive Metals in Tribocorrosion Systems. *J. Electrochem. Soc.* **1998**, *145*, 750. [[CrossRef](#)]
23. Takadoum, J. The influence of potential on the tribocorrosion of nickel and iron in sulfuric acid solution. *Corros. Sci.* **1996**, *38*, 643–654. [[CrossRef](#)]
24. Li, J.; Yang, B.B.; Lu, Y.H.; Xin, L.; Wang, Z.H.; Shoji, T. The effects of electrochemical polarization condition and applied potential on tribocorrosion behaviors of Inconel 690 alloys in water environment. *Mater. Des.* **2017**, *119*, 93–103. [[CrossRef](#)]
25. Hua, N.; Chen, W.; Wang, Q.; Guo, Q.; Huang, Y.; Zhang, T. Tribocorrosion behaviors of a biodegradable Mg65Zn30Ca5 bulk metallic glass for potential biomedical implant applications. *J. Alloys Compd.* **2018**, *745*, 111–120. [[CrossRef](#)]
26. Liu, S.; Li, G.; Qi, Y.; Peng, Z.; Ye, Y.; Liang, J. Corrosion and tribocorrosion resistance of MAO-based composite coating on AZ31 magnesium alloy. *J. Magnes. Alloys* **2022**, *10*, 3406–3417. [[CrossRef](#)]
27. Siddaiah, A.; Mao, B.; Kasar, A.K.; Liao, Y.; Menezes, P.L. Influence of laser shock peening on the surface energy and tribocorrosion properties of an AZ31B Mg alloy. *Wear* **2020**, *462–463*, 203490. [[CrossRef](#)]
28. Günen, A. Tribocorrosion behavior of boronized Co<sub>1.19</sub>Cr<sub>1.86</sub>Fe<sub>1.30</sub>Mn<sub>1.39</sub>Ni<sub>1.05</sub>Al<sub>0.17</sub>B<sub>0.04</sub> high entropy alloy. *Surf. Coat. Technol.* **2021**, *421*, 127426. [[CrossRef](#)]
29. Karakaş, M.S.; Günen, A.; Çarboğa, C.; Karaca, Y.; Demir, M.; Altınay, Y.; Erdoğan, A. Microstructure, some mechanical properties and tribocorrosion wear behavior of boronized Al<sub>0.07</sub>Co<sub>1.26</sub>Cr<sub>1.80</sub>Fe<sub>1.42</sub>Mn<sub>1.35</sub>Ni<sub>1.10</sub> high entropy alloy. *J. Alloys Compd.* **2021**, *886*, 161222. [[CrossRef](#)]
30. Zeng, Q.; Xu, Y. A comparative study on the tribocorrosion behaviors of AlFeCrNiMo high entropy alloy coatings and 304 stainless steel. *Mater. Today Commun.* **2020**, *24*, 101261. [[CrossRef](#)]
31. Fu, Y.; Huang, C.; Du, C.; Li, J.; Dai, C.; Luo, H.; Liu, Z.; Li, X. Evolution in microstructure, wear, corrosion, and tribocorrosion behavior of Mo-containing high-entropy alloy coatings fabricated by laser cladding. *Corros. Sci.* **2021**, *191*, 109727. [[CrossRef](#)]
32. Ayyagari, A.; Barthelemy, C.; Gwalani, B.; Banerjee, R.; Scharf, T.W.; Mukherjee, S. Reciprocating sliding wear behavior of high entropy alloys in dry and marine environments. *Mater. Chem. Phys.* **2018**, *210*, 162–169. [[CrossRef](#)]
33. Hua, N.; Wang, W.; Wang, Q.; Ye, Y.; Lin, S.; Zhang, L.; Guo, Q.; Brechtel, J.; Liaw, P.K. Mechanical, corrosion, and wear properties of biomedical Ti–Zr–Nb–Ta–Mo high entropy alloys. *J. Alloys Compd.* **2021**, *861*, 157997. [[CrossRef](#)]
34. Huttunen-Saarivirta, E.; Isotahdon, E.; Metsäjoki, J.; Salminen, T.; Carpén, L.; Ronkainen, H. Tribocorrosion behaviour of aluminium bronze in 3.5 wt.% NaCl solution. *Corros. Sci.* **2018**, *144*, 207–223. [[CrossRef](#)]
35. Alkan, S.; Gök, M.S. Effect of sliding wear and electrochemical potential on tribocorrosion behaviour of AISI 316 stainless steel in seawater. *Eng. Sci. Technol. Int. J.* **2021**, *24*, 524–532. [[CrossRef](#)]
36. Henry, P.; Takadoum, J.; Berçot, P. Tribocorrosion of 316L stainless steel and TA6V4 alloy in H<sub>2</sub>SO<sub>4</sub> media. *Corros. Sci.* **2009**, *51*, 1308–1314. [[CrossRef](#)]
37. Jemmely, P.; Mischler, S.; Landolt, D. Tribocorrosion behaviour of Fe–17Cr stainless steel in acid and alkaline solutions. *Tribol. Int.* **1999**, *32*, 295–303. [[CrossRef](#)]
38. Diomidis, N.; Celis, J.P.; Ponthiaux, P.; Wenger, F. Tribocorrosion of stainless steel in sulfuric acid: Identification of corrosion–wear components and effect of contact area. *Wear* **2010**, *269*, 93–103. [[CrossRef](#)]
39. Liang, D.D.; Wei, X.S.; Ma, T.C.; Chen, B.; Jiang, H.R.; Dong, Y.; Shen, J. Sliding tribocorrosion behavior of Fe-based bulk metallic glass under corrosive environments. *J. Non-Cryst. Solids* **2019**, *510*, 62–70. [[CrossRef](#)]
40. Hassani, S.; Raeissi, K.; Azzi, M.; Li, D.; Golozar, M.A.; Szpunar, J.A. Improving the corrosion and tribocorrosion resistance of Ni–Co nanocrystalline coatings in NaOH solution. *Corros. Sci.* **2009**, *51*, 2371–2379. [[CrossRef](#)]
41. Hacısalıhoğlu, I.; Samancıoğlu, A.; Yıldız, F.; Purçek, G.; Alsarın, A. Tribocorrosion properties of different type titanium alloys in simulated body fluid. *Wear* **2015**, *332–333*, 679–686. [[CrossRef](#)]
42. Albayrak, Ç.; Hacısalıhoğlu, İ.; Yenil Vangölü, S.; Alsarın, A. Tribocorrosion behavior of duplex treated pure titanium in Simulated Body Fluid. *Wear* **2013**, *302*, 1642–1648. [[CrossRef](#)]
43. Manhabosco, T.M.; Tamborim, S.M.; dos Santos, C.B.; Müller, I.L. Tribological, electrochemical and tribo-electrochemical characterization of bare and nitrided Ti6Al4V in simulated body fluid solution. *Corros. Sci.* **2011**, *53*, 1786–1793. [[CrossRef](#)]
44. Igual Muñoz, A.; Mischler, S. Effect of the environment on wear ranking and corrosion of biomedical CoCrMo alloys. *J. Mater. Sci. Mater. Med.* **2011**, *22*, 437–450. [[CrossRef](#)]
45. More, N.S.; Diomidis, N.; Paul, S.N.; Roy, M.; Mischler, S. Tribocorrosion behavior of  $\beta$  titanium alloys in physiological solutions containing synovial components. *Mater. Sci. Eng. C* **2011**, *31*, 400–408. [[CrossRef](#)]
46. Wang, Z.; Zhou, Y.; Wang, H.; Li, Y.; Huang, W. Tribocorrosion behavior of Ti-30Zr alloy for dental implants. *Mater. Lett.* **2018**, *218*, 190–192. [[CrossRef](#)]

47. Naghibi, S.A.; Raeissi, K.; Fathi, M.H. Corrosion and tribocorrosion behavior of Ti/TiN PVD coating on 316L stainless steel substrate in Ringer's solution. *Mater. Chem. Phys.* **2014**, *148*, 614–623. [[CrossRef](#)]
48. Wang, Z.; Huang, W.; Li, Y.; He, H.; Zhou, Y.; Zheng, Z. Tribocorrosion behaviour of a biomedical Ti-25Nb-3Mo-3Zr-2Sn alloy in Ringer's solution. *Mater. Sci. Eng. C* **2017**, *76*, 1094–1102. [[CrossRef](#)] [[PubMed](#)]
49. Mraied, H.; Cai, W. The effects of Mn concentration on the tribocorrosion resistance of Al–Mn alloys. *Wear* **2017**, *380–381*, 191–202. [[CrossRef](#)]
50. Ferreira, S.C.; Sequeira, P.D.; Watanabe, Y.; Ariza, E.; Rocha, L.A. Microstructural characterization and tribocorrosion behaviour of Al/Al<sub>3</sub>Ti and Al/Al<sub>3</sub>Zr FGMs. *Wear* **2011**, *270*, 806–814. [[CrossRef](#)]
51. Jamaati, R.; Toroghinejad, M.R.; Szpunar, J.A.; Li, D. Tribocorrosion Behavior of Aluminum/Alumina Composite Manufactured by Anodizing and ARB Processes. *J. Mater. Eng. Perform.* **2011**, *20*, 1600–1605. [[CrossRef](#)]
52. Toptan, F.; Alves, A.C.; Kerti, I.; Ariza, E.; Rocha, L.A. Corrosion and tribocorrosion behaviour of Al–Si–Cu–Mg alloy and its composites reinforced with B<sub>4</sub>C particles in 0.05M NaCl solution. *Wear* **2013**, *306*, 27–35. [[CrossRef](#)]
53. Karabacak, A.H.; Çanakçı, A.; Erdemir, F.; Özkaya, S.; Çelebi, M. Corrosion and Mechanical Properties of Novel AA2024 Matrix Hybrid Nanocomposites Reinforced with B<sub>4</sub>C and SiC Particles. *Silicon* **2022**, *14*, 8567–8579. [[CrossRef](#)]
54. Cheng, J.; Ge, Y.; Wang, B.; Zhang, L.; Hu, X.; Hong, S.; Liang, X.; Zhang, X. Microstructure and Tribocorrosion Behavior of Al<sub>2</sub>O<sub>3</sub>/Al Composite Coatings: Role of Al<sub>2</sub>O<sub>3</sub> Addition. *J. Therm. Spray Technol.* **2020**, *29*, 1741–1751. [[CrossRef](#)]
55. Gnanavelbabu, A.; Amul, X.J.; Surendran, K.T.S. Investigation on the tribocorrosion and electrochemical corrosion behaviour of AA2014/Al<sub>2</sub>O<sub>3</sub> nanocomposites fabricated through ultrasonication coupled stir-squeeze casting method. *J. Appl. Electrochem.* **2022**, *52*, 765–791. [[CrossRef](#)]
56. Xu, L.; Liu, W.; Li, J.; Dong, M.; Ma, F.; Wang, C.; Wang, L. Effect of heat treatment on tribocorrosion behavior of 7B05 aluminum alloy in artificial seawater. *Mater. Res. Express* **2019**, *6*, 106598. [[CrossRef](#)]
57. Zhao, H.; Cao, L.; Wan, Y.; Pu, J. Effect of sodium octanoate on the tribocorrosion behaviour of 5052 aluminium alloy. *Tribol.-Mater. Surf. Interfaces* **2018**, *12*, 200–207. [[CrossRef](#)]
58. Pokhmurskii, V.; Zin, I.; Vynar, V.; Khlopyk, O.; Bily, L. Corrosive wear of aluminium alloy in presence of phosphate. *Corros. Eng. Sci. Technol.* **2012**, *47*, 182–187. [[CrossRef](#)]
59. Vieira, A.C.; Rocha, L.A.; Papageorgiou, N.; Mischler, S. Mechanical and electrochemical deterioration mechanisms in the tribocorrosion of Al alloys in NaCl and in NaNO<sub>3</sub> solutions. *Corros. Sci.* **2012**, *54*, 26–35. [[CrossRef](#)]
60. Liu, Y.; Mol, J.M.C.; Janssen, G. Combined Corrosion and Wear of Aluminium Alloy 7075-T6. *J. Bio-Tribo-Corros.* **2016**, *2*, 9. [[CrossRef](#)]
61. Li, Z.; Yu, H.; Wen, L.; Sun, D. Influence of Applied Load and Sliding Velocity on Tribocorrosion Behavior of 7075-T6 Aluminum Alloy. *Metals* **2022**, *12*, 1626. [[CrossRef](#)]
62. Chen, J.; Cai, W. Effect of scratching frequency on the tribocorrosion resistance of Al–Mn amorphous thin films. *Wear* **2019**, *426–427*, 1457–1465. [[CrossRef](#)]
63. Jun, C.; Bingli, P.; Quanan, L. Tribocorrosion Behavior of LY12 Aluminum Alloy in Artificial Seawater Solution. *Tribol. Trans.* **2020**, *63*, 1085–1094. [[CrossRef](#)]
64. Li, Z.; Yu, H.; Sun, D. The tribocorrosion mechanism of aluminum alloy 7075-T6 in the deep ocean. *Corros. Sci.* **2021**, *183*, 109306. [[CrossRef](#)]
65. Archard, J.F. Contact and rubbing of flat surfaces. *J. Appl. Phys.* **1953**, *24*, 981–988. [[CrossRef](#)]
66. Geanta, V.V.V. Chemical composition influence on microhardness, microstructure and phase morphology of Al<sub>x</sub>CrFeCoNi high entropy alloys. *Rev. Chim.* **2018**, *69*, 798–801. [[CrossRef](#)]
67. Cai, W.; Mabon, J.; Bellon, P. Crystallographic textures and texture transitions induced by sliding wear in bronze and nickel. *Wear* **2009**, *267*, 485–494. [[CrossRef](#)]
68. Jiru, M.G.; Singh, B. Surface engineered AlMn alloy using laser surface alloying for wear resistance. *Int. J. Adv. Manuf. Technol.* **2020**, *110*, 275–281. [[CrossRef](#)]
69. Dubourg, L.; Pelletier, H.; Vaissiere, D.; Hlawka, F.; Cornet, A. Mechanical characterisation of laser surface alloyed aluminium–copper systems. *Wear* **2002**, *253*, 1077–1085. [[CrossRef](#)]
70. Du, J.; Yang, Y.; Ren, Y.; Wu, H.; Shan, Q.; Wu, X.; Lu, Y.; Baker, I. A crack-free Ti-modified Al–Cu alloy processed by in-situ alloying laser powder bed fusion: Tribological behaviors and mechanical properties. *J. Alloys Compd.* **2023**, *960*, 170549. [[CrossRef](#)]
71. Wu, J.-M.; Lin, S.-J.; Yeh, J.-W.; Chen, S.-K.; Huang, Y.-S.; Chen, H.-C. Adhesive wear behavior of Al<sub>x</sub>CoCrCuFeNi high-entropy alloys as a function of aluminum content. *Wear* **2006**, *261*, 513–519. [[CrossRef](#)]
72. Yu, Y.; Wang, J.; Li, J.-S.; Kou, H.-C.; Niu, S.-Z.; Zhu, S.-Y.; Yang, J.; Liu, W.-M. Dry-sliding tribological properties of AlCoCrFeNiTi<sub>0.5</sub> high-entropy alloy. *Rare Met.* **2022**, *41*, 4266–4272. [[CrossRef](#)]
73. Dai, Y.; Yan, L.; Hao, J. Review on Micro-Alloying and Preparation Method of 7xxx Series Aluminum Alloys: Progresses and Prospects. *Materials* **2022**, *15*, 1216. [[CrossRef](#)]
74. De Rosso, E.; dos Santos, C.A.; Garcia, A. Microstructure, Hardness, Tensile Strength, and Sliding Wear of Hypoeutectic Al–Si Cast Alloys with Small Cr Additions and Fe-Impurity Content. *Adv. Eng. Mater.* **2022**, *24*, 2001552. [[CrossRef](#)]
75. Farhat, Z.N.; Ding, Y.; Northwood, D.O.; Alpas, A.T. Effect of grain size on friction and wear of nanocrystalline aluminum. *Mater. Sci. Eng.* **1996**, *206*, 302–313.

76. Pochet, P.; Bellon, P.; Chaffron, L.; Martin, G. Phase transformations under ball milling: Theory versus experiment. *Mater. Sci. Forum* **1996**, *225*, 207–216. [[CrossRef](#)]
77. Chee, S.W.; Stumphy, B.; Vo, N.Q.; Averback, R.S.; Bellon, P. Dynamic self-organization in Cu alloys under ion irradiation. *Acta Mater.* **2010**, *58*, 4088–4099. [[CrossRef](#)]
78. Singh, J.; Alpas, A.T. Dry Sliding Wear Mechanisms in a Ti50Ni47Fe3 Intermetallic Alloy. *Wear* **1995**, *181*, 302–311. [[CrossRef](#)]
79. Kasai, T.; Fu, X.Y.; Rigney, D.A.; Zharin, A.L. Applications of a non-contacting Kelvin probe during sliding. *Wear* **1999**, *229*, 1186–1204. [[CrossRef](#)]
80. Baumberger, T.; Caroli, C. Solid friction from stick-slip down to pinning and aging. *Adv. Phys.* **2006**, *55*, 279–348. [[CrossRef](#)]
81. Cai, W.; Bellon, P. Subsurface microstructure evolution and deformation mechanism of Ag–Cu eutectic alloy after dry sliding wear. *Wear* **2013**, *303*, 602–610. [[CrossRef](#)]
82. Singh, J.B.; Wen, J.G.; Bellon, P. Nanoscale characterization of the transfer layer formed during dry sliding of Cu–15wt.% Ni–8wt.% Sn bronze alloy. *Acta Mater.* **2008**, *56*, 3053–3064. [[CrossRef](#)]
83. Chu, K.; Zhu, W.; Zhao, C.; Ren, F. Forced atomic mixing of immiscible Nb–Ag Alloys by severe plastic deformation. *Mater. Lett.* **2017**, *207*, 141–144. [[CrossRef](#)]
84. Jasim, K.M.; Dwarakadasa, E.S. Wear in Al–Si Alloys under Dry Sliding Conditions. *Wear* **1987**, *119*, 119–130. [[CrossRef](#)]
85. Dubourg, L.; Hlawka, F.; Cornet, A. Study of aluminium-copper-iron alloys: Application for laser cladding. *Surf. Coat. Technol.* **2002**, *151*, 329–332. [[CrossRef](#)]
86. Liu, X.; Zeng, M.Q.; Ma, Y.; Zhu, M. Wear behavior of Al–Sn alloys with different distribution of Sn dispersoids manipulated by mechanical alloying and sintering. *Wear* **2008**, *265*, 1857–1863. [[CrossRef](#)]
87. Cai, W.; Schuh, C.A. Tuning nanoscale grain size distribution in multilayered Al–Mn alloys. *Scr. Mater.* **2012**, *66*, 194–197. [[CrossRef](#)]
88. Jeng, Y.R.; Tsai, P.C.; Chiang, S.H. Effects of grain size and orientation on mechanical and tribological characterizations of nanocrystalline nickel films. *Wear* **2013**, *303*, 262–268. [[CrossRef](#)]
89. Vargel, C. *Corrosion of Aluminium*; Elsevier: Amsterdam, The Netherlands, 2004.
90. Szklarska-Smialowska, Z. Pitting corrosion of aluminum. *Corros. Sci.* **1999**, *41*, 1743–1767. [[CrossRef](#)]
91. Gudic, S.; Smoljko, I.; Kliskic, M. The effect of small addition of tin and indium on the corrosion behavior of aluminium in chloride solution. *J. Alloys Compd.* **2010**, *505*, 54–63. [[CrossRef](#)]
92. Kim, Y.; Buchheit, R.G. A characterization of the inhibiting effect of Cu on metastable pitting in dilute Al–Cu solid solution alloys. *Electrochim. Acta* **2007**, *52*, 2437–2446. [[CrossRef](#)]
93. Mraied, H.; Cai, W.; Sagüés, A.A. Corrosion resistance of Al and Al–Mn thin films. *Thin Solid Film.* **2016**, *615*, 391–401. [[CrossRef](#)]
94. Petrunin, M.A.; Maksaeva, L.B.; Yurasova, T.A. The role of acid–base interactions in the pitting corrosion of aluminum: A review. *Corros. Rev.* **2023**, *41*, 515–535. [[CrossRef](#)]
95. Natishan, P.M.; O’Grady, W.E. Chloride Ion Interactions with Oxide-Covered Aluminum Leading to Pitting Corrosion: A Review. *J. Electrochem. Soc.* **2014**, *161*, C421. [[CrossRef](#)]
96. Foley, R.T. Localized Corrosion of Aluminum-Alloys—A Review. *Corrosion* **1986**, *42*, 277–288. [[CrossRef](#)]
97. Lavanya, M.; Ghosal, J.; Rao, P. A comprehensive review of corrosion inhibition of aluminium alloys by green inhibitors. *Can. Metall. Q.* **2023**. [[CrossRef](#)]
98. Olugbade, T.O. Review: Corrosion Resistance Performance of Severely Plastic Deformed Aluminium Based Alloys via Different Processing Routes. *Met. Mater. Int.* **2023**, *29*, 2415–2443. [[CrossRef](#)]
99. Bryant, M.G.; Buente, D.; Oladokun, A.; Ward, M.; Huber, G.; Morlock, M.; Neville, A. Surface and subsurface changes as a result of tribocorrosion at the stem-neck interface of bi-modular prosthesis. *Biotribology* **2017**, *10*, 1–16. [[CrossRef](#)]
100. Ralston, K.D.; Fabijanic, D.; Birbilis, N. Effect of grain size on corrosion of high purity aluminium. *Electrochim. Acta* **2011**, *56*, 1729–1736. [[CrossRef](#)]
101. Ralston, K.D.; Birbilis, N. Effect of Grain Size on Corrosion: A Review. *Corrosion* **2010**, *66*, 075005. [[CrossRef](#)]
102. Son, I.J.; Nakano, H.; Oue, S.; Kobayashi, S.; Fukushima, H.; Horita, Z. Pitting corrosion resistance of ultrafine-grained aluminum processed by severe plastic deformation. *Mater. Trans.* **2006**, *47*, 1163–1169. [[CrossRef](#)]
103. Balyanov, A.; Kutnyakova, J.; Amirkhanova, N.A.; Stolyarov, V.V.; Valiev, R.Z.; Liao, X.Z.; Zhao, Y.H.; Jiang, Y.B.; Xu, H.F.; Lowe, T.C.; et al. Corrosion resistance of ultra fine-grained Ti. *Scr. Mater.* **2004**, *51*, 225–229. [[CrossRef](#)]
104. Huang, R.; Han, Y. The effect of SMAT-induced grain refinement and dislocations on the corrosion behavior of Ti–25Nb–3Mo–3Zr–2Sn alloy. *Mat. Sci. Eng. C-Mater.* **2013**, *33*, 2353–2359. [[CrossRef](#)]
105. Wang, X.Y.; Li, D.Y. Mechanical and electrochemical behavior of nanocrystalline surface of 304 stainless steel. *Electrochim. Acta* **2002**, *47*, 3939–3947. [[CrossRef](#)]
106. Wang, X.Y.; Li, D.Y. Mechanical, electrochemical and tribological properties of nano-crystalline surface of 304 stainless steel. *Wear* **2003**, *255*, 836–845. [[CrossRef](#)]
107. Orłowska, M.; Ura-Bińczyk, E.; Olejnik, L.; Lewandowska, M. The effect of grain size and grain boundary misorientation on the corrosion resistance of commercially pure aluminium. *Corros. Sci.* **2019**, *148*, 57–70. [[CrossRef](#)]
108. Mahmoud, T.S. Effect of friction stir processing on electrical conductivity and corrosion resistance of AA6063–T6 Al alloy. *Proc. Inst. Mech. Eng. C-J. Mech.* **2008**, *222*, 1117–1123. [[CrossRef](#)]

109. Hockauf, M.; Meyer, L.W.; Nickel, D.; Alisch, G.; Lampke, T.; Wielage, B.; Kruger, L. Mechanical properties and corrosion behaviour of ultrafine-grained AA6082 produced by equal-channel angular pressing. *J. Mater. Sci.* **2008**, *43*, 7409–7417. [[CrossRef](#)]
110. Eizadjou, M.; Fattahi, H.; Talachi, A.K.; Manesh, H.D.; Janghorban, K.; Shariat, M.H. Pitting corrosion susceptibility of ultrafine grains commercially pure aluminium produced by accumulative roll bonding process. *Corros. Eng. Sci. Technol.* **2012**, *47*, 19–24. [[CrossRef](#)]
111. Osorio, W.R.; Freire, C.M.; Garcia, A. The role of macrostructural morphology and grain size on the corrosion resistance of Zn and Al castings. *Mat. Sci. Eng. A-Struct.* **2005**, *402*, 22–32. [[CrossRef](#)]
112. Faghihi, S.; Li, D.; Szpunar, J.A. Tribocorrosion behaviour of nanostructured titanium substrates processed by high-pressure torsion. *Nanotechnology* **2010**, *21*, 485703. [[CrossRef](#)]
113. Wang, H.; Estrin, Y.; Fu, H.; Song, G.; Zuberova, Z. The effect of pre-processing and grain structure on the bio-corrosion and fatigue resistance of magnesium alloy AZ31. *Adv. Eng. Mater.* **2007**, *9*, 967–972. [[CrossRef](#)]
114. Song, D.; Ma, A.B.; Jiang, J.H.; Lin, P.H.; Yang, D.H.; Fan, J.F. Corrosion behavior of equal-channel-angular-pressed pure magnesium in NaCl aqueous solution. *Corros. Sci.* **2010**, *52*, 481–490. [[CrossRef](#)]
115. Glaeser, W.; Wright, I.G. Forms of Mechanically Assisted Degradation. In *Corrosion: Fundamentals, Testing, and Protection*; ASM International: Novelty, OH, USA, 2003.
116. Oltra, R. *Electrochemical Aspects of Localized Depassivation during Abrasion of Passive Iron-Based Alloys in Acidic Media*; The Minerals, Metals and Materials Society: Warrendale, PA, USA, 1991.
117. Kim, Y.; Buchheit, R.G.; Kotula, P.G. Effect of alloyed Cu on localized corrosion susceptibility of Al-Cu solid solution alloys—Surface characterization by XPS and STEM. *Electrochim. Acta* **2010**, *55*, 7367–7375. [[CrossRef](#)]
118. Sanchette, F.; Ducros, C.; Billard, A.; Rébéré, C.; Berziou, C.; Reffass, M.; Creus, J. Nanostructured aluminium based coatings deposited by electron-beam evaporative PVD. *Thin Solid Film.* **2009**, *518*, 1575–1580. [[CrossRef](#)]
119. Merl, D.K.; Panjan, P.; Milosev, I. Effect of tungsten content on properties of PVD sputtered Al-W-X alloys. *Surf. Eng.* **2013**, *29*, 281–286. [[CrossRef](#)]
120. Tekin, K.C.; Malayoglu, U. Assessing the Tribocorrosion Performance of Three Different Nickel-Based Superalloys. *Tribol. Lett.* **2010**, *37*, 563–572. [[CrossRef](#)]
121. Perret, J.; Boehm-Courjault, E.; Cantoni, M.; Mischler, S.; Beaudouin, A.; Chitty, W.; Vernot, J.P. EBSD, SEM and FIB characterisation of subsurface deformation during tribocorrosion of stainless steel in sulphuric acid. *Wear* **2010**, *269*, 383–393. [[CrossRef](#)]
122. Doni, Z.; Alves, A.C.; Toptan, F.; Gomes, J.R.; Ramalho, A.; Buciumeanu, M.; Palaghian, L.; Silva, F.S. Dry sliding and tribocorrosion behaviour of hot pressed CoCrMo biomedical alloy as compared with the cast CoCrMo and Ti6Al4V alloys. *Mater. Des.* **2013**, *52*, 47–57. [[CrossRef](#)]
123. Martin, E.; Azzi, M.; Salishchev, G.A.; Szpunar, J. Influence of microstructure and texture on the corrosion and tribocorrosion behavior of Ti-6Al-4V. *Tribol. Int.* **2010**, *43*, 918–924. [[CrossRef](#)]
124. Chuang, M.-H.; Tsai, M.-H.; Wang, W.-R.; Lin, S.-J.; Yeh, J.-W. Microstructure and wear behavior of Al<sub>x</sub>Co<sub>1.5</sub>CrFeNi<sub>1.5</sub>Ti<sub>y</sub> high-entropy alloys. *Acta Mater.* **2011**, *59*, 6308–6317. [[CrossRef](#)]
125. Lahiri, D.; Gill, P.K.; Scudino, S.; Zhang, C.; Singh, V.; Karthikeyan, J.; Munroe, N.; Seal, S.; Agarwal, A. Cold sprayed aluminum based glassy coating: Synthesis, wear and corrosion properties. *Surf. Coat. Technol.* **2013**, *232*, 33–40. [[CrossRef](#)]
126. Fang, Q.; Huang, Z.; Li, L.; Huang, Z.; Liu, B.; Liu, Y.; Li, J.; Liaw, P.K. Modeling the competition between solid solution and precipitate strengthening of alloys in a 3D space. *Int. J. Plast.* **2022**, *149*, 103152. [[CrossRef](#)]
127. Zupanič, F.; Bončina, T.; Suštaršič, B.; Anžel, I.; Markoli, B. Microstructure of Al–Mn–Be melt-spun ribbons. *Mater. Charact.* **2008**, *59*, 1245–1251. [[CrossRef](#)]
128. Song, G.; Fleury, E.; Kim, S.; Kim, W.; Kim, D. Formation and Stability of Quasicrystalline and Hexagonal Approximant Phases in an Al–Mn–Be Alloy. *J. Mater. Res.* **2002**, *17*, 1671–1677. [[CrossRef](#)]
129. Ruan, S.; Schuh, C.A. Electrodeposited Al-Mn alloys with microcrystalline, nanocrystalline, amorphous and nano-quasicrystalline structures. *Acta Mater.* **2009**, *57*, 3810–3822. [[CrossRef](#)]
130. Merl, D.K.; Panjan, P.; Kovač, J. Corrosion and surface study of sputtered Al-W coatings with a range of tungsten contents. *Corros. Sci.* **2013**, *69*, 359–368. [[CrossRef](#)]
131. Creus, J.; Billard, A.; Sanchette, F. Corrosion behaviour of amorphous Al-Cr and Al-Cr-(N) coatings deposited by dc magnetron sputtering on mild steel substrate. *Thin Solid Film* **2004**, *466*, 1–9. [[CrossRef](#)]
132. Creus, J.; Berziou, C.; Cohendoz, S.; Perez, A.; Rébéré, C.; Reffass, M.; Touzain, S.; Allely, C.; Gachon, Y.; Héau, C.; et al. Reactivity classification in saline solution of magnetron sputtered or EB-PVD pure metallic, nitride and Al-based alloy coatings. *Corros. Sci.* **2012**, *57*, 162–173. [[CrossRef](#)]
133. Perez, A.; Billard, A.; Rébéré, C.; Berziou, C.; Touzain, S.; Creus, J. Influence of metallurgical states on the corrosion behaviour of Al-Zn PVD coatings in saline solution. *Corros. Sci.* **2013**, *74*, 240–249. [[CrossRef](#)]
134. Bielawski, M. Development of unbalanced magnetron sputtered Al-Mo coatings for cadmium replacement. *Surf. Coat. Technol.* **2004**, *179*, 10–17. [[CrossRef](#)]
135. Frankel, G.S.; Russak, M.A.; Jahnes, C.V.; Mirzamaani, M.; Brusic, V.A. Pitting of Sputtered Aluminum Alloy Thin Films. *J. Electrochem. Soc.* **1989**, *136*, 1243–1244. [[CrossRef](#)]
136. Car, T.; Radić, N.; Panjan, P.; Čekada, M.; Tonejc, A. Correlation between hardness and stress in Al-(Nb, Mo, Ta) thin films. *Thin Solid Film* **2009**, *517*, 4605–4609. [[CrossRef](#)]

137. Chen, J.; Xiao, J.; Poplawsky, J.; Michel, F.M.; Deng, C.; Cai, W. The origin of passivity in aluminum-manganese solid solutions. *Corros. Sci.* **2020**, *173*, 108749. [[CrossRef](#)]
138. Reffass, M.; Berziou, C.; Rébéré, C.; Billard, A.; Creus, J. Corrosion behaviour of magnetron-sputtered Al<sub>1-x</sub>Mn<sub>x</sub> coatings in neutral saline solution. *Corros. Sci.* **2010**, *52*, 3615–3623. [[CrossRef](#)]
139. Chen, J.; Xiao, J.; Hung, C.-Y.; Wang, W.; Zhao, J.; Marc Michel, F.; Deng, C.; Cai, W. Effects of alloying concentration on the aqueous corrosion and passivation of aluminum-manganese-molybdenum concentrated alloys. *Corros. Sci.* **2022**, *198*, 110137. [[CrossRef](#)]
140. Izadi, S.; Mraied, H.; Cai, W. Tribological and mechanical behavior of nanostructured Al/Ti multilayers. *Surf. Coat. Technol.* **2015**, *275*, 374–383. [[CrossRef](#)]
141. Cai, W.; Schuh, C.A. Microstructure and mechanical properties of electrodeposited Al<sub>1-x</sub>Mn<sub>x</sub>/Al<sub>1-y</sub>Mn<sub>y</sub> nanostructured multilayers. *J. Mater. Res.* **2014**, *29*, 2229–2239. [[CrossRef](#)]
142. Wang, W.; Wang, K.; Zhang, Z.; Chen, J.; Mou, T.; Michel, F.M.; Xin, H.; Cai, W. Ultrahigh tribocorrosion resistance of metals enabled by nano-layering. *Acta Mater.* **2021**, *206*, 116609. [[CrossRef](#)]
143. Wang, K.; Cai, W. Modeling the effects of individual layer thickness and orientation on the tribocorrosion behavior of Al/Cu nanostructured metallic multilayers. *Wear* **2021**, *477*, 203849. [[CrossRef](#)]
144. Sun, X.; Mraied, H.; Cai, W.; Zhang, Q.; Liang, G.; Li, M. Bayesian latent degradation performance modeling and quantification of corroding aluminum alloys. *Reliab. Eng. Syst. Saf.* **2018**, *178*, 84–96. [[CrossRef](#)]
145. Madapana, D.; Bathe, R.; Manna, I.; Dutta Majumdar, J. Tribocorrosion Behaviour of Laser-Induced Periodic Surface Structured Ti6Al4V. *J. Bio-Tribo-Corros.* **2023**, *9*, 9. [[CrossRef](#)]
146. Griffiths, R.J.; Garcia, D.; Song, J.; Vasudevan, V.K.; Steiner, M.A.; Cai, W.; Yu, H.Z. Solid-state additive manufacturing of aluminum and copper using additive friction stir deposition: Process-microstructure linkages. *Materialia* **2021**, *15*, 100967. [[CrossRef](#)]
147. Wang, K.; Zhang, Z.; Dandu, R.S.B.; Cai, W. Understanding Tribocorrosion of Aluminum at the Crystal Level. *Acta Mater.* **2023**, *245*, 118639. [[CrossRef](#)]
148. Fanijo, E.O.; Thomas, J.G.; Zhu, Y.; Cai, W.; Brand, A.S. Surface Characterization Techniques: A Systematic Review of their Principles, Applications, and Perspectives in Corrosion Studies. *J. Electrochem. Soc.* **2022**, *169*, 111502. [[CrossRef](#)]
149. Mraied, H.; Wang, W.B.; Cai, W.J. Influence of chemical heterogeneity and microstructure on the corrosion resistance of biodegradable WE43 magnesium alloys. *J. Mater. Chem. B* **2019**, *7*, 6399–6411. [[CrossRef](#)]
150. Wang, W.; Mraied, H.; Diyatmika, W.; Chu, J.P.; Li, L.; Cai, W. Effects of nanoscale chemical heterogeneity on the wear, corrosion, and tribocorrosion resistance of Zr-based thin film metallic glasses. *Surf. Coat. Technol.* **2020**, *402*, 126324. [[CrossRef](#)]
151. Cai, W.; Bellon, P. Microstructural self-organization triggered by twin boundaries during dry sliding wear. *Acta Mater.* **2012**, *60*, 6673–6684. [[CrossRef](#)]
152. Chen, L.; Chen, Y.; Yang, H.; Su, Y.; Qiao, L. Study of the relationship between intergranular stress corrosion cracking and grain boundary characteristics in brass. *Electrochem. Commun.* **2021**, *131*, 107124. [[CrossRef](#)]
153. Wang, W.; Kattoura, M.; Bovid, S.; Zhang, Z.; Lahrman, D.; Cai, W. Effects of nanosecond laser shock peening on residual stress, corrosion and tribocorrosion behavior of WE43 magnesium alloys. *Wear* **2023**, *524–525*, 204866. [[CrossRef](#)]
154. Wang, W.; Tamakloe, S.; Deng, Z.; Li, L.; Cai, W.; Lu, K. Effects of processing temperature on the corrosion and tribocorrosion resistance of perhydropolysilazane-derived coatings on AISI 304 steel. *Surf. Coat. Technol.* **2022**, *439*, 128463. [[CrossRef](#)]
155. Zhang, Z.; Yao, Y.; Liu, L.; Mou, T.; Xin, H.; Li, L.; Cai, W. Computational design of non-equiatomic CoCrFeNi alloys towards optimized mechanical and surface properties. *J. Mater. Res.* **2022**, *37*, 2738–2748. [[CrossRef](#)]
156. Yao, Y.; Zhang, Z.; Cai, W.; Li, L. Atomistic investigations of Cr effect on the deformation mechanisms and mechanical properties of CrCoFeNi alloys. *J. Appl. Phys.* **2023**, *133*, 195103. [[CrossRef](#)]
157. Wang, K.; Wang, Y.; Yue, X.; Cai, W. Multiphysics modeling and uncertainty quantification of tribocorrosion in aluminum alloys. *Corros. Sci.* **2021**, *178*, 109095. [[CrossRef](#)]
158. Wang, Y.; Wang, K.; Cai, W.; Yue, X. NP-ODE: Neural process aided ordinary differential equations for uncertainty quantification of finite element analysis. *IJSE Trans.* **2022**, *54*, 211–226. [[CrossRef](#)]
159. Lee, C.; Wang, K.; Wu, J.; Cai, W.; Yue, X. Partitioned Active Learning for Heterogeneous Systems. *J. Comput. Inf. Sci. Eng.* **2023**, *23*, 041009. [[CrossRef](#)]
160. Kılınc, M.; Elen, L.; Ahlatcı, H.; Sun, Y.; Türen, Y.; Acarer, M. Investigation of a New Type of Aluminum–Magnesium Alloy with Bismuth Additions Subjected to Thermomechanical Heat Treatment. *Int. J. Met.* **2023**. [[CrossRef](#)]
161. Ekaputra, C.N.; Rakhmonov, J.U.; Weiss, D.; Mogonye, J.-E.; Dunand, D.C. Microstructure and mechanical properties of cast Al-Ce-Sc-Zr-(Er) alloys strengthened by Al<sub>11</sub>Ce<sub>3</sub> micro-platelets and L<sub>12</sub> Al<sub>3</sub>(Sc,Zr,Er) nano-precipitates. *Acta Mater.* **2022**, *240*, 118354. [[CrossRef](#)]
162. El-Hadad, S.; Moussa, M.E.; Shoeib, M. Influence of Al<sub>11</sub>Ce<sub>3</sub> Size and Distribution on the Electrochemical Properties of Sonoprocessed Al-10 wt.% Ce Alloy. *Int. J. Met.* **2023**, *17*, 1606–1614. [[CrossRef](#)]
163. Wang, W.; Pan, Q.; Lin, G.; Wang, X.; Sun, Y.; Wang, X.; Ye, J.; Sun, Y.; Yu, Y.; Jiang, F.; et al. Microstructure and properties of novel Al-Ce-Sc, Al-Ce-Y, Al-Ce-Zr and Al-Ce-Sc-Y alloy conductors processed by die casting, hot extrusion and cold drawing. *J. Mater. Sci. Technol.* **2020**, *58*, 155–170. [[CrossRef](#)]

164. Deillon, L.; Jensch, F.; Palm, F.; Bambach, M. A new high strength Al–Mg–Sc alloy for laser powder bed fusion with calcium addition to effectively prevent magnesium evaporation. *J. Mater. Process. Technol.* **2022**, *300*, 117416. [[CrossRef](#)]
165. Jeyaprakash, N.; Yang, C.-H.; Kumar, M.S. Influence of coherent intermetallic nano-precipitates on the nano-level mechanical and tribological properties of the Laser-Powder bed fused Scalmalloy. *Mater. Charact.* **2022**, *193*, 112269. [[CrossRef](#)]
166. Wu, X.; Lv, Y. Study on the Corrosion Resistance of Laser Clad Al0.7FeCoCrNiCux High-Entropy Alloy Coating in Marine Environment. *Coatings* **2022**, *12*, 1855. [[CrossRef](#)]
167. Zhang, Z.; Zhang, S.; Lu, N.; Chen, Y.; Liang, X. Study on Tribocorrosion Behaviors of AlNiZr Amorphous and Nanocrystalline Composite Coatings. *China Mech. Eng.* **2022**, *33*, 1435–1443.
168. Jia, Y.; Su, R.; Wang, L.; Li, G.; Qu, Y.; Li, R. Study on Microstructure and Properties of AA2024-T6I4 with Deep Cryogenic Treatment. *Trans. Indian Inst. Met.* **2023**, *76*, 741–748. [[CrossRef](#)]
169. Dai, G.; Xue, M.; Guo, Y.; Sun, Z.; Chang, H.; Lu, J.; Li, W.; Panwisawas, C.; Alexandrov, I.V. Gradient microstructure and strength-ductility synergy improvement of 2319 aluminum alloys by hybrid additive manufacturing. *J. Alloys Compd.* **2023**, *968*, 171781. [[CrossRef](#)]
170. Fu, L.; Li, X.; Lin, L.; Wang, Z.; Zhang, Y.; Luo, Y.; Yan, S.; He, C.; Wang, Q. Study on Microstructure Evolution Mechanism of Gradient Structure Surface of AA7075 Aluminum Alloy by Ultrasonic Surface Rolling Treatment. *Materials* **2023**, *16*, 5616. [[CrossRef](#)]
171. Li, W.L.; Tao, N.R.; Lu, K. Fabrication of a gradient nano-micro-structured surface layer on bulk copper by means of a surface mechanical grinding treatment. *Scr. Mater.* **2008**, *59*, 546–549. [[CrossRef](#)]
172. Beura, V.K.; Karanth, Y.; Darling, K.; Solanki, K. Role of gradient nanograined surface layer on corrosion behavior of aluminum 7075 alloy. *npj Mater. Degrad.* **2022**, *6*, 62. [[CrossRef](#)]
173. David, A.; Gopal, S.K.; Lakshmanan, P.; Chenbagam, A.S. Corrosion, mechanical and microstructural properties of aluminum 7075—Carbon nanotube nanocomposites for robots in corrosive environments. *Int. J. Miner. Metall. Mater.* **2023**, *30*, 1140–1151. [[CrossRef](#)]
174. Chen, S.N.; Yan, W.Q.; Liao, B.; Wu, X.Y.; Chen, L.; Ouyang, X.; Ouyang, X.P. Effect of temperature on the tribocorrosion and high-temperature tribological behaviour of strong amorphization AlCrNiTiV high entropy alloy film in a multifactor environment. *Ceram. Int.* **2023**, *49*, 6880–6890. [[CrossRef](#)]
175. Nisar, M.; Charoo, M.S. A Comparative Analysis of Corrosion Performance of Piston Alloy and Its Composite in Marine, Mining and Basic Environments. *J. Bio- Tribo-Corros.* **2022**, *8*, 42. [[CrossRef](#)]

**Disclaimer/Publisher’s Note:** The statements, opinions and data contained in all publications are solely those of the individual author(s) and contributor(s) and not of MDPI and/or the editor(s). MDPI and/or the editor(s) disclaim responsibility for any injury to people or property resulting from any ideas, methods, instructions or products referred to in the content.